In presenting the dissertation as a partial fulfillment of the requirements for an advanced degree from the Georgia Institute of Technology, I agree that the Library of the Institute shall make it available for inspection and circulation in accordance with its regulations governing materials of this type. I agree that permission to copy from, or to publish from, this dissertation may be granted by the professor under whose direction it was written, or, in his absence, by the Dean of the Graduate Division when such copying or publication is solely for scholarly purposes and does not involve potential financial gain. It is understood that any copying from, or publication of, this dissertation which involves potential financial gain will not be allowed without written permission.

7/25/68

ELECTRONIC MOVEMENTS IN METALS UNDER STRESS

A THESIS

Presented to

The Faculty of the Graduate Division

by

John Yun-Shoa Liu

In Partial Fulfillment

of the Requirements for the Degree

Master of Science in Metallurgy

Georgia Institute of Technology

March, 1970

ELECTRONIC MOVEMENTS IN METALS UNDER STRESS

Approved:

Chairman

Date approved by Chairman: May 25-70

ACKNOWLEDGMENTS

The author takes great pleasure in acknowledging the contributions of those who have assisted him in developing and presenting this study.

To Dr. Niels N. Engel I extend my particular gratitude and appreciation. Dr. Engel suggested the research topic and served as chairman of the Thesis Reading Committee. Without his teaching, consultation, and experience this work would not have been possible.

A great deal of appreciation is also extended to Dr. Stephen Spooner for his help and advice on the preparation of the manuscript and to Dr. Helen Grenga for her review of the manuscript.

Finally, the author would like to give special thanks to his wife, Gloria, for her love, encouragement, and understanding.

TABLE OF CONTENTS

LIST OF TABLES

LIST OF FIGURES

LIST OF FIGURES

SUMMARY

This research is based on Engel theory correlating crystal structure and electron concentration. The purpose of this research is an attempt to measure the movements of electrons between outer shells and inner shells associated with uniaxial stress and three-axial compression. It is divided in two sections: one concerned measurements under uniaxial stress dealt with in this paper and another one concerned with compression carried out by another student. The present part of the investigation is carried out by measuring the adiabatic heats under stressing of the elements in the periodic chart except those elements which were too brittle or too costly. The present work is restricted to the effect in uniaxial tension. These measurements, together with measurements in three-axial compression, promise to yield the necessary information for final conclusions.

CHAPTER I

SURVEY OF BONDING THEORIES

Atoms in solid crystals are held together by various kinds of forces which may be roughly divided into three types: the van der Waal's bond, the ionic bond, and the covalent bond including the metallic bond.

Firstly, van der Waal considered the van der Waal's forces which are explained as being due to nonsymmetrical charge distributions. These forces can be ascribed to the interactions of electrical dipoles. A van der Waal's bond arises because there are at any one time a few more electrons on one side of the nucleus than on the other side; the centers of positive and negative charge do not coincide and thus dipoles are produced. A force then exists between opposite ends of dipoles in adjacent atoms or molecules which tends to draw them together. This type of force, which exists even between neutral atoms, is usually quite small and of short range, compared to chemical bonding as covalent metallic and ionic bonds. When chemical bonding occurs between all atoms in a solid, the van der Waal's forces have little influence on determining the arrangements of groups of atoms. They determine the lattice in most molecular compounds, as for example organic solids.

In a structure held together by ionic bonds, electrons have been transferred from one kind of atom to another. Charged particles called

ions thus are formed and the main forces within the structure take two basic forms. One force is an electrostatic attraction that varies inversely with the square of the distance and is nondirectional. The other force is a repulsion that occurs when ions are brought so close together that outer electronic shells begin to overlap. Ionic lattices are arranged in such a manner that the distance between opposite charged ions is minimum and the distance between equally charged ions is kept as great as possible. An equilibrium spacing between oppositely charged ions is obtained when electrostatic attractive and shell overlap repulsive forces are in balance. This theory was developed by Born (1) and Madelung (2).

In general, atoms bonded by nondirectional bonds usually obey certain geometrical rules affected by their difference in size. The greater the size difference, the smaller the coordination number. In ionic crystals, the anions and cations usually differ appreciably in size. For example, the NaCl lattice has a coordination number of six, while CsCl lattice has a coordination number of eight because the former differs more in size than the latter. In general, the more favorable the size factor is, the higher coordination number is expected.

In the sodium chloride lattice, the positive and negative ions both carry the same valence. However, ionic structures can also be formed from atoms that have different valences, for instance, $BeCl_2$ or Al_2O_3. The ions in the above two cases have filled electronic shells after the electron transfer. But cases exist in which unfilled shell ions form structures, such as CuO and UO_2.

In a covalent bond, the linking force is built up by electron sharing, each atom contributing one or more electrons to the bond. In molecules, atoms are added until filled electronic shells are formed in all the atoms by means of electron sharing. Thus, carbon, with four valence electrons per atom, crystallizes in diamond lattice with four nearest neighbors, so that each carbon atom has a total of eight shared electrons. In the same manner, arsenic, antimony, and bismuth, which have five valency electrons per atom, need to share electrons with three neighbors in order to attain the eight electrons needed for a closed shell configuration in each atom. Therefore these elements crystallized with three nearest neighbors. Many elemental covalent crystals follow the Hume-Rothery (8-N) rule (3), where N is the number of valency electrons, and the factor (8-N) gives the number of nearest neighbors in the structure. The covalent bond theory, proposed by G. N. Lewis in 1916 (4,5), has been applied widely and with great success in organic and inorganic chemistry.

Many theories have been proposed to explain the metallic properties. These can be divided into two major groups. One is the electron gas theory with its many variations and the other is the electron pairing theory.

The electron gas theory was developed in three stages. The early conception of an electron gas in the metallic state, advanced by Drude and Lorentz (6), assumed that the outer electrons of the atoms were ionized off and formed an "electron gas" which diffused through a lattice formed by positively charged metal ions, as shown in Figure 1. The

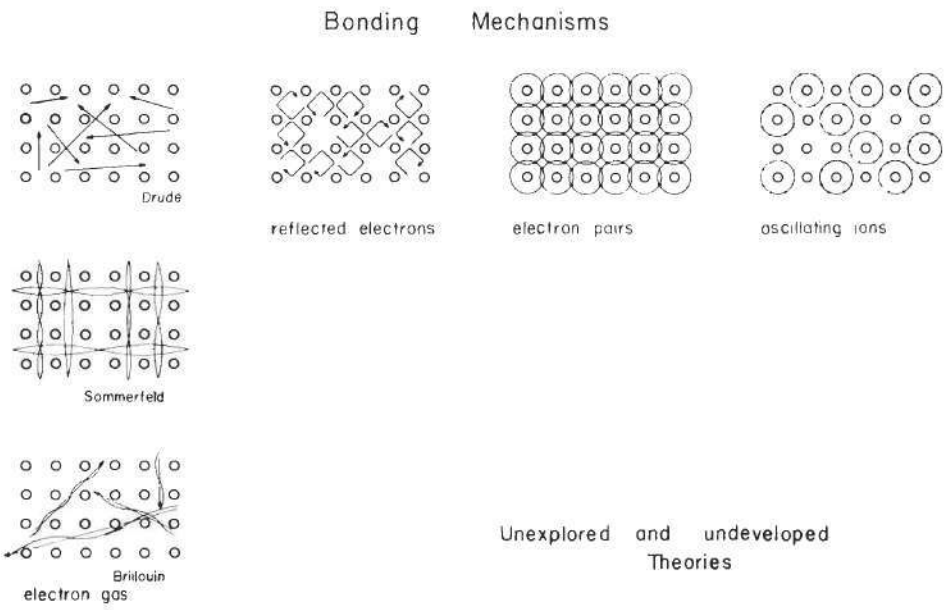

Figure 1. Bonding Mechanisms in the Metals

theory accounted for the conductivity of metals, but it could not explain the difference between a conductor and an insulator. Nor could the theory predict the experimental values of the specific heats of the elements.

To overcome this difficulty, Sommerfeld (7) introduced the principle of quantum mechanics. On this basis, the valency electrons are assumed to belong to the whole crystal structure, and the energy levels of the electrons become rearranged when the solid is formed. In the Sommerfeld theory, it is also assumed that the potential in which an electron moves inside a metal is constant, as shown in Figure 1. The greatest success of the Sommerfeld theory is its ability to explain why the electronic contribution to the specific heat is so small. However, the theory was still unable to explain the difference between conductors and insulators, the cause of the magnetic properties of metals, or the connection between the characteristic metallic crystal structure types and the electron concentration in metals.

A further development in the electron gas theory was made by Bloch (8), who suggested that the valency electrons move in a periodical potential field, as demonstrated in Figure 1. One important result derived from these assumptions is that the electrons are able to move in any direction with a corresponding variety of velocities in the metal lattice except for the restrictions imposed on them by the Brillouin zones and the boundaries of the metallic lattice.

One of the successes of the band theory is its ability to distinguish conductors from insulators. In the metals possessing high

electrical and thermal conductivity, the electron energy bands within the Brillouin zone are only partly filled with electrons. The electrons can move under an external influence, e.g. an electrostatic field. In the case when an energy band in a crystal is completely filled and separated from the next band by a forbidden-energy region, the electrons cannot undergo transitions to adjacent quantum states and the crystal is an insulator.

The mathematical treatments of the band theory may be found in the textbooks by Seitz (9), Pauling (10), Mott and Jones (11) and others. Although the band theory is widely accepted by solid state physicists, there are still some serious shortcomings and discrepancies between experimental fact and the band theory. Therefore a better theory of bonding mechanism is needed and desired.

One of those shortcomings is that the character of s, p, d, and f electrons in free atoms is lost when the bonding electrons enter a solid phase and the specific behavior of electrons cannot be calculated, except with great difficulty. According to Bohr's theory of atomic structures, the electrons in a free atom can occupy different quantum states, and each electronic state in a given atom gives rise to a definite electron density, which is characterized by a definite energy and a definite set of quantum numbers, n, l, m_l, and m_s. For example, in atoms with only one outer bonding electron available per atom, this electron will be an s electron in its ground state. According to calculation carried out by Pauling, s electrons are distributed symmetrically around the nuclei like a hollow sphere. The p, d, and f electrons have similar

specific characteristics, one of which is a fixed location of the orbit or the electron density pattern. According to the band theory, however, all the bonding electrons move in different directions within a Brillouin zone. If this were the only physics being taken into account, there would be no characteristic shape of single bonding electrons. As a consequence, all the lattices of metals might be expected to be a close packed lattice. Obviously this theory is inadequate to describe the facts.

In summary, the electron gas theory was developed in an effort to obtain a mathematical model that would fit the experimental data. However, there are a great number of points in which the physical interpretation of the mathematics is impossible.

In 1916, G. N. Lewis (4), recognizing the stability of the filled electron shell, proposed the electron pairing theory. Later the quantum mechanics has been applied to the concept of covalent bonding by Heisenberg (13) in 1925 and Schrodinger (14) in 1926. However, the electron pairing theory has not received as much attention as the electron gas theory. In 1949, Engel (15) elaborated the electron pairing concept and applied it to the metallic properties, such as electrical conductivity, metallic lattice structure, cohesive energy, melting points, phase diagrams (12), and so on.

According to the electron pairing theory, the interatomic forces are due to the sharing of electron pairs. All electrons unpaired in the free atom become paired when lattices or molecules are formed. This kind of atomic linkage due to electron sharing is called homopolar or

covalent bonding. The main difference between electron pairing theory and electron gas theory is that according to the electron pairing theory, the bonding electrons maintain their specific character, such as size and shape of orbit and energy level in forming bonds, whereas the electrons according to the electron gas concept enter new quantum states in which the electrons are quantized to the entire molecule or lattice. The fixed electronic energy levels appear lower due to the energy liberated by pairing and may be different for s, p, or d electrons. According to the electron gas theory, the energy levels of s, p, and d electrons on the Fermi surface are amalgamated into a band of energies.

It is generally accepted that each free atom has a fixed and well defined pattern of quantum states. Engel has postulated that these quantum states are essentially unchangable. Engel asserts that electronic quantum states correlated to many ions cannot exist as simple moving electrons since no quantum states can develop on potential tops or ridges. Electrons must jump from one quantum state to another. If such electronic transitions create more bonding electrons, some electrons remain in excited states for the purpose of forming more bonds. Bonding between atoms, then, is postulated to be due to the formation of electron pairs. The forces and mechanisms causing electrons to enter quantum states and to form pairs can be accounted for on the basis a particle model according to which moving particles are visualized as long snake-like structures rather than points or balls (16).

When there are too few electrons in an extended lattice to build up filled shells in all atoms, permanent electronic vacancies will remain.

The electronic vacancies are responsible for the conduction properties. In this case, electrons are able to transfer from a quantum state in one atom to the vacant quantum state at the same energy level in another atom. If all the electronic shells are filled in extended three dimensional lattices, the material exhibits insulator properties. The mechanism of electronic conduction may be seen in Figure 2 where several electronic orbits are depicted. The electrons are shown as long snake-like structures which enter quantum states with path lengths equal to an integer of the mass wavelength. When an electron moves from a quantum state in one atom to a similar one in another atom, it must unwind out of the old quantum state and wind up at the new place. Because of the finite velocity of the electrons, the uncoiling and recoiling during a jump takes a finite time. During this time the donor and accepter atoms are linked together with a stiff connection because of the fixed mass wavelength of the quantized electron. Therefore, the electrical and thermal conduction are linked together.

Regarding electrons in quantum states as rigid oscillators, the electron oscillator theory was introduced by Engel (15), who recognized the different effects of bonding electrons in s, p, d, and f states. On this basis, Engel has postulated that there is a correlation between the number of bonding electrons and the lattices of the metals. It is postulated that the body centered cubic lattice is a one electron per atom phase, that the hexagonal close packed lattice is a two electrons per atom phase, and that the face centered cubic lattice is a three electrons per atom phase. For transition metals, all unpaired d-electrons

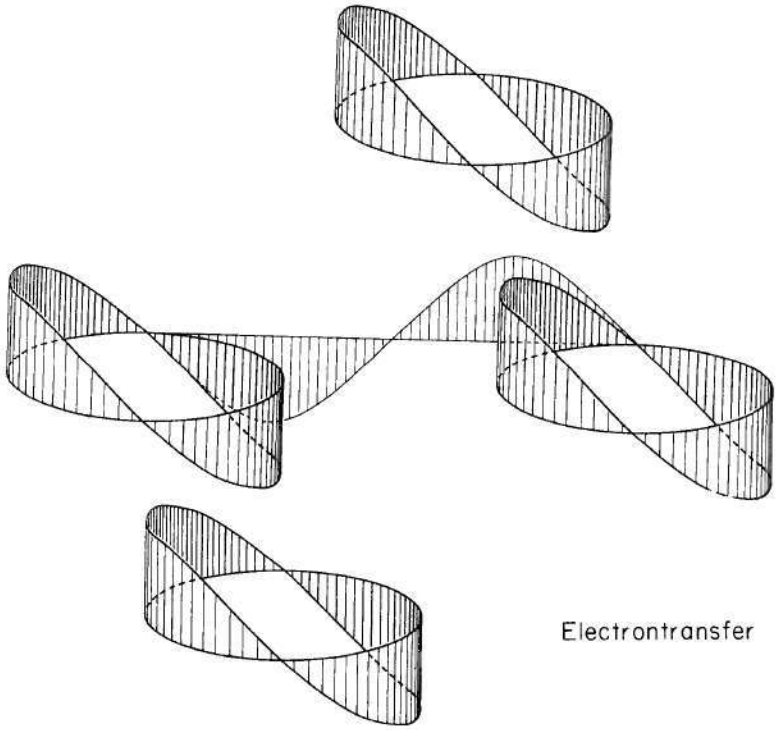

Figure 2. The Mechanism of Electronic Conduction

take part in the bonding process, but they play no part in controlling the type of crystal structure, which is determined solely by the number of outer electrons (15,17). These correlations have been used to account for the distribution of lattices in the periodic chart (15). For example, in the fifth period, Rb, Nb, and Mo have an electron concentration around one and exhibit the body centered cubic lattice Sr, Y, Zr, Tc, Ru, and Cd have two outer electrons per atom and crystallize with hexagonal close packed lattices and Rh, Pd, Ag, and In with three outer electrons per atom have face centered lattices. The lattices in other periods are also determined by the electron concentration of the outer electrons.

The Engel correlations can also be used in reverse and the electron concentration may be determined from the lattices. The thermodynamic properties of the elements over the periodic chart can be explained by the electron pairing theory. As illustrated in Figures 3, 4, and 5, the peaks of melting point curves appear in the middle of the transition elements, sixth column, and in the middle of the normal elements, fourteenth column. The body centered cubic lattices of the sixth column elements are in agreement with this postulate according to which there should be one outer electron. The d electron shell in the sixth column elements are consequently half filled, that is, all five d electrons are unpaired and take part in bonding. Five unpaired d electrons is the highest number obtainable. Therefore the highest bonding strength and melting point are expected in the sixth column. In the fourteenth column elements, there are four outer electrons per

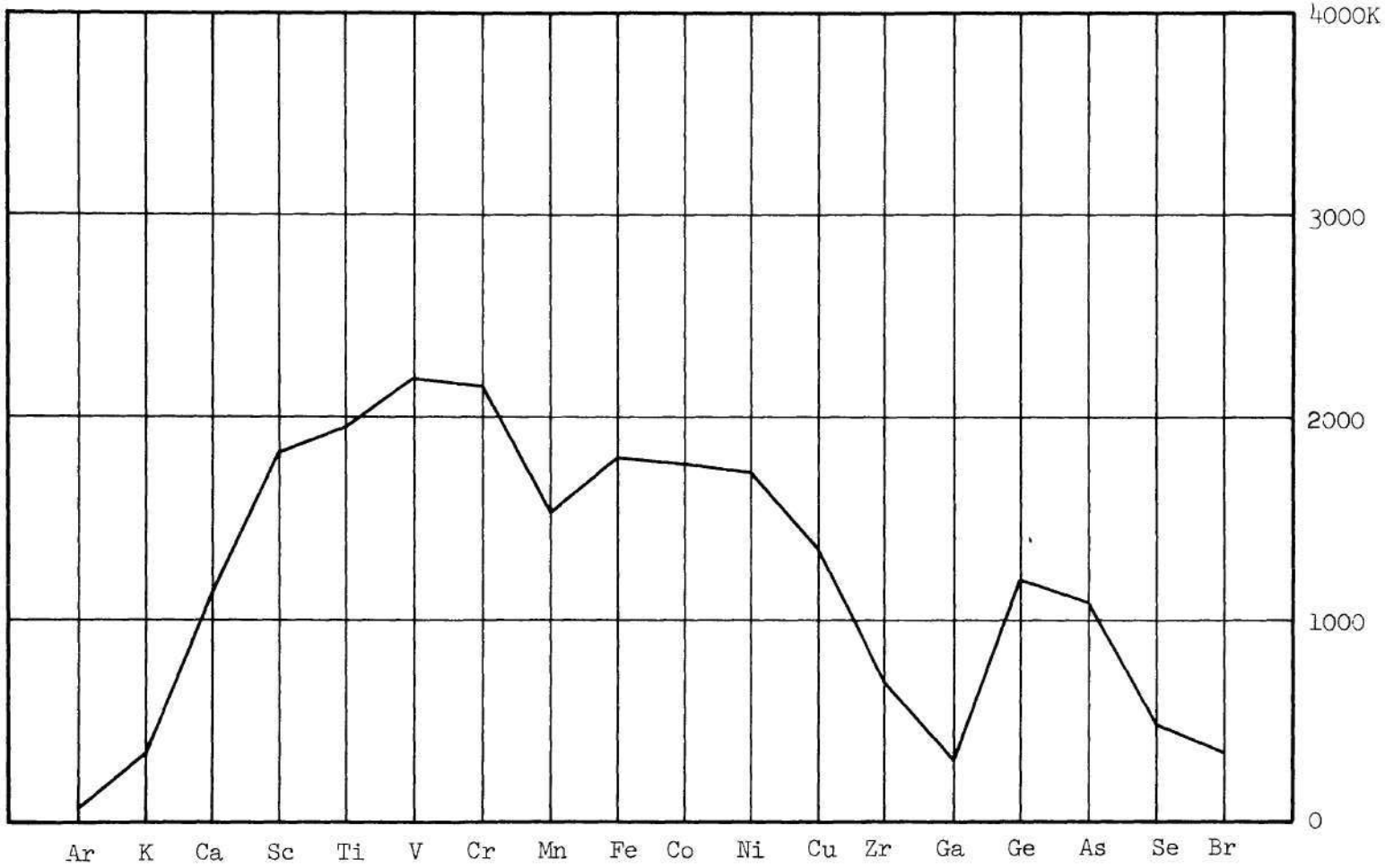

Figure 3. Melting Point of the Fourth Period Elements

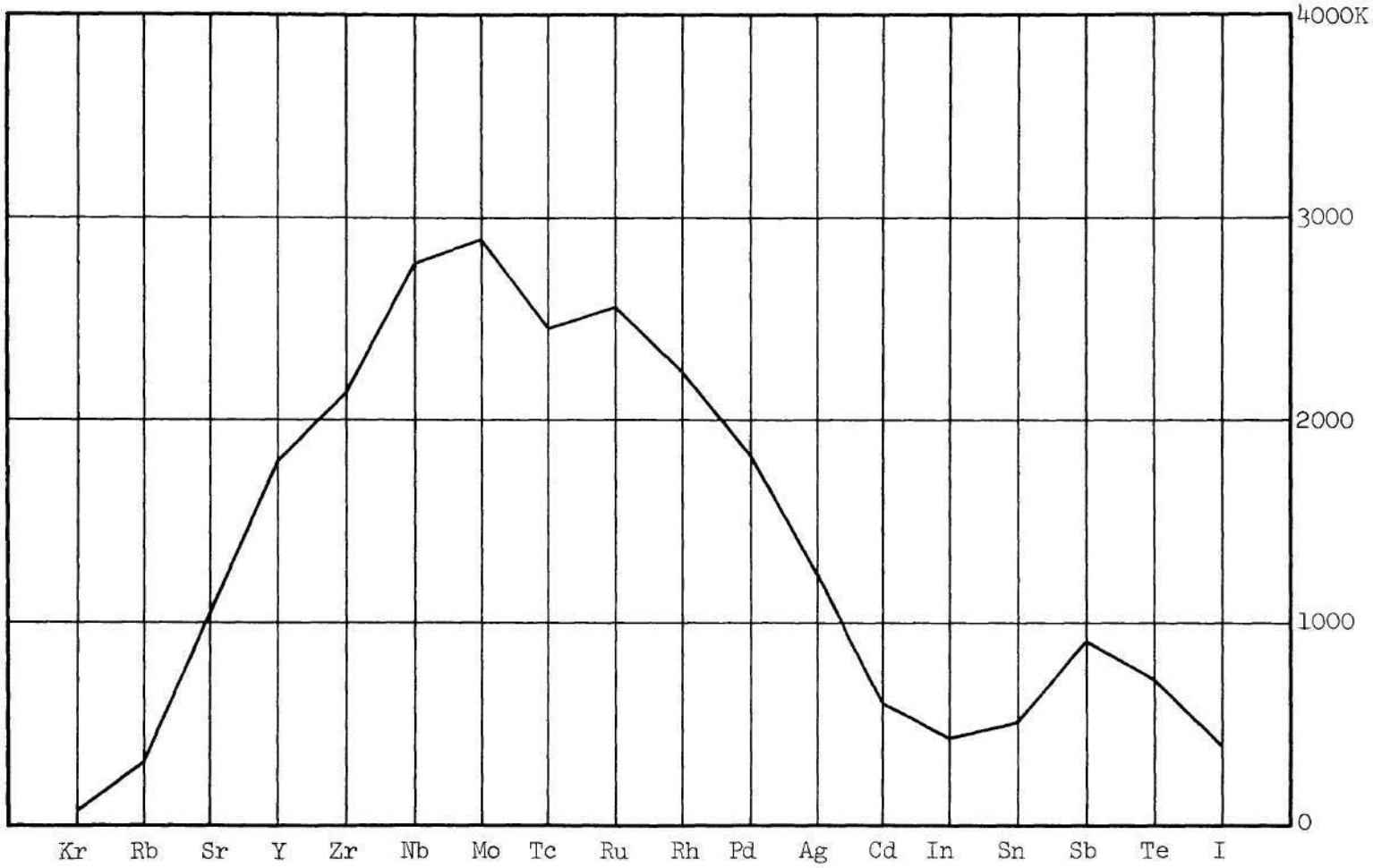

Figure 4. Melting Point of the Fifth Period Elements

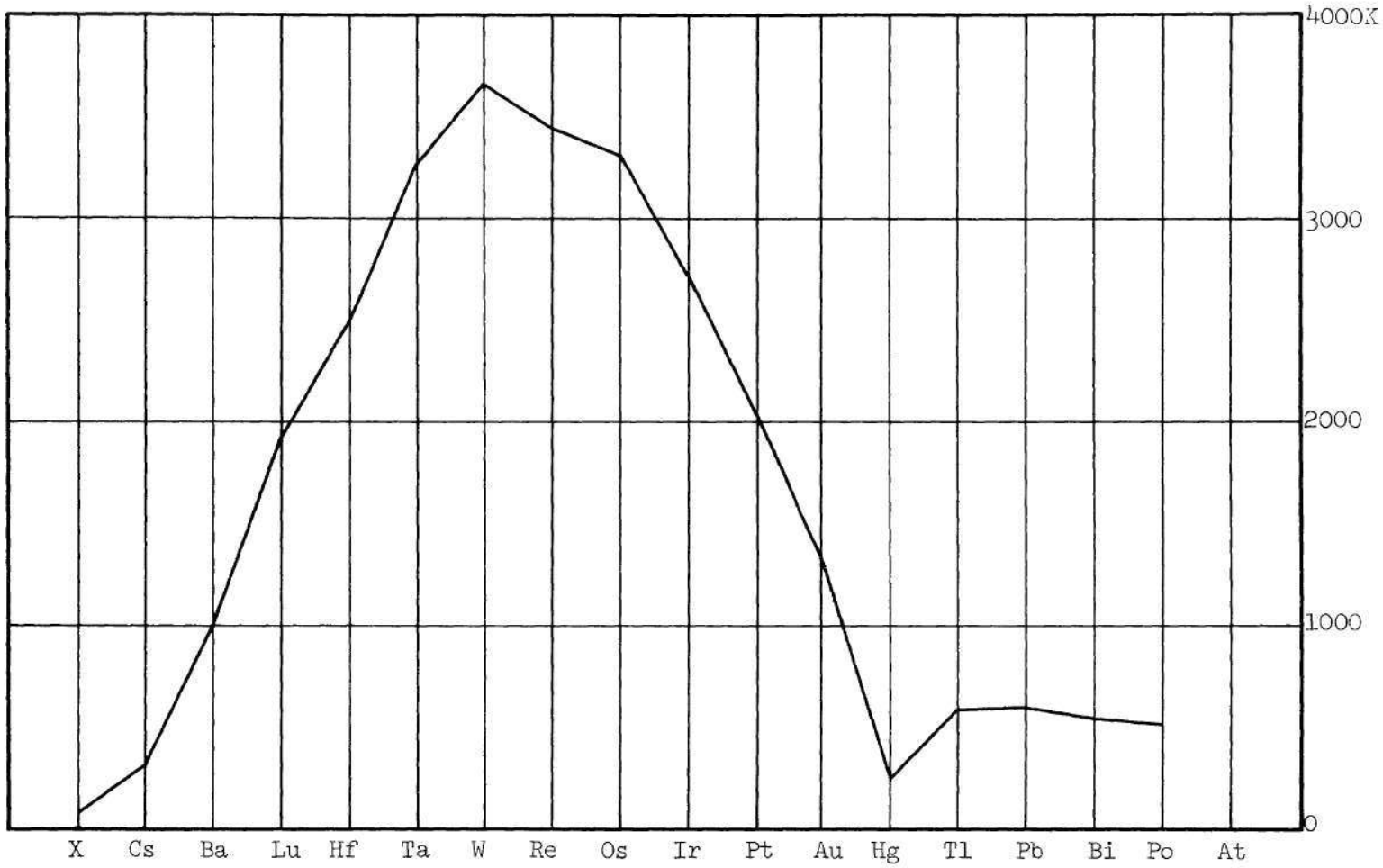

Figure 5. Melting Point of the Sixth Period Elements

atom participating in bonding and no d-electrons. Since four covalent bonds in normal elements are the highest number that can be formed, the peaks in melting points and bonding strength in normal elements have the appearance shown in the fourteenth column.

The electron pairing theory can be used to explain many facts, including the Hume-Rothery (8-N) rule, atomic size, and the organic and inorganic structural rules. Furthermore, Engel theory explains the lattice distribution over the periodic chart in terms of electron concentration as well as conduction properties.

The present investigation is an attempt to check the Engel theory. According to the electron gas theory, the upper energy levels should be the same for all electrons (s, p, and d). The energy levels and orbit sizes of the different shells of bonding electrons differ according to the Engel theory. Compression or tension could therefore be expected to give an observable thermal effect according to the Engel theory predictions described in the following chapter.

CHAPTER II

THEORETICAL APPROACH

In the Engel theory, both the s+p electrons and d electrons participate into the bonding between atoms of pure transition elements. Since the outer s+p electrons preferentially form bonds with s+p electrons and d electrons make the strongest bonds with other d electrons, the half filled d shell (five unpaired d electrons) will yield the highest bonding strength. This is the result of the postulate that the bonding electrons maintain their specific size and shape of orbit and energy level in free atom as well as in bonded condition in the solid state. The fixed electronic energy levels appear lower due to the energy liberated by pairing. The atomic distance in solid state could therefore be considered to be controlled by both the outer electron and inner electron characteristics. Present investigations are based on the above assumption.

Figures 6, 7, and 8 show the atomic distance variation over fourth, fifth, and sixth period. The thick line curves indicate the actual atomic distance. The upper curves give a calculated atomic distance if bonding were only controlled by s electrons. The lower curves show a calculated atomic distance assuming there were only d electrons determining atomic distances. Consider the example in Figure 7. The calculation for the upper curve is based on the assumption that

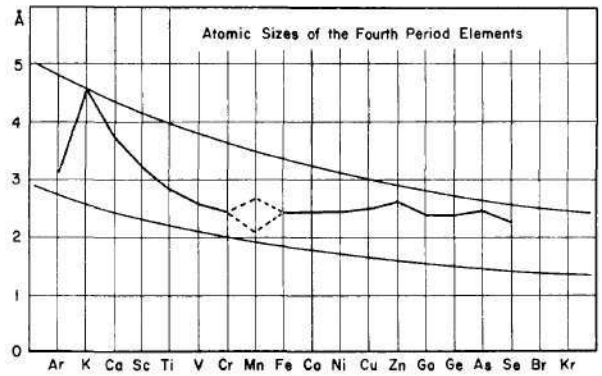

Figure 6. Atomic Distance of the Fourth Period Elements

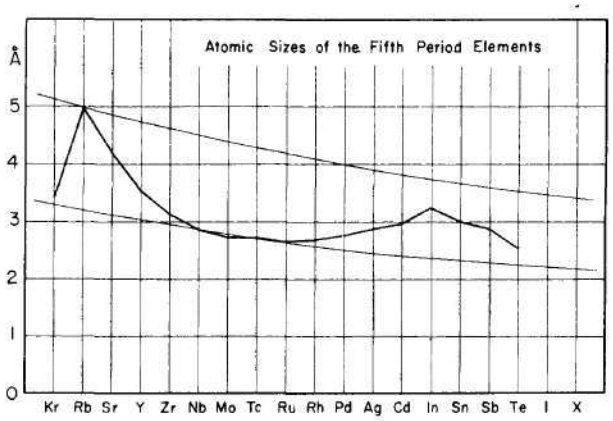

Figure 7. Atomic Distance of the Fifth Period Elements

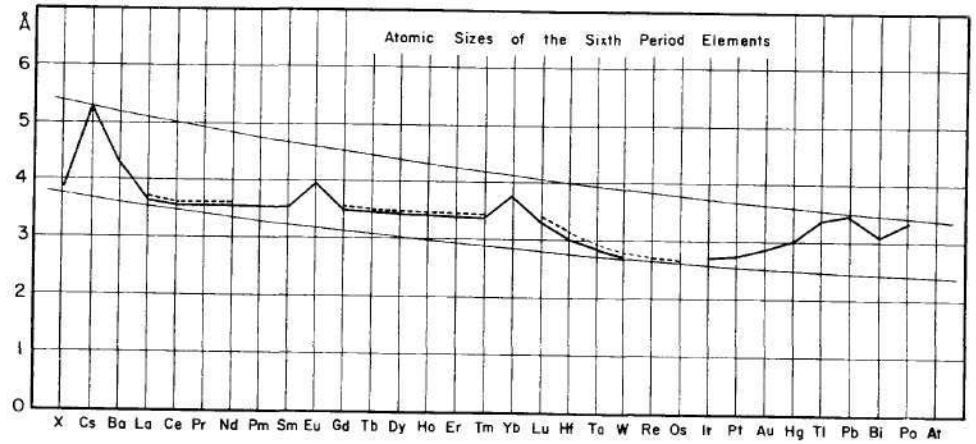

Figure 8. Atomic Distance of the Sixth Period Elements

the atomic distance contracts with increasing nuclear charge. Since Rb is the first element in the fifth period, it is reasonable to assume one s electron in the fifth shell and no d electrons in the fourth shell. If only s electrons were to participate in bonding, the atomic distance of each element in the fifth period could be calculated from the atomic distance of Rb by the relationship $\frac{Rs\ 37}{Z}$, where Rs is the atomic distance in the solid and 37 is the atomic number of Rb. Z is the atomic number of each element through the fifth period. The calculated values of each element in the fifth period are shown as the upper curve in Figure 7. If only d electrons were to participate in bonding, the atomic distance could be computed in a similar manner by the relationship $\frac{Rs\ 37}{Z}\frac{4^2}{5^2}$, where 4 and 5 are the principal quantum numbers for the d-electrons in the fourth shell and the s-electrons in the fifth shell, respectively. The d-shell sizes are shown as the lower curve in Figure 7. The curves of atomic distance with only s+p electrons and only d electrons participating in bonding are obtained by similar calculations for the fourth and the sixth periods as shown in Figures 6 and 8.

According to Engel theory, in column 6 (Cr, Mo, and W) where there are one outer and five d bonding electrons, the highest bonding strength appears in this column. As illustrated in Figures 6, 7, and 8, the actual atomic distances of Cr, Mo, and W are rather close to the lower curves, which are calculated from the assumption there were only d electrons participating in bonding. The actual atomic distances of the remaining elements vary and are located between the upper curves and the lower curves in each period. In other words, the atomic distances

of K, Rb, and Cs are controlled solely by s-electron bonding, whereas the atomic distances of Cr, Mo, and W are controlled by d electron bonding. The intermediate atomic distances are affected by both outer s+p electrons and inner d electrons. The actual distance between atoms will depend on the number of outer electrons and inner electrons. It is assumed that the distribution of electrons between outer and inner shells is controlled by the electronic structure of the free atoms, the promotion energy required to move the electrons between the outer shell and the inner shell, and the bonding energy.

It is known that the thermal energy influences the interatomic distance and sometimes the lattice structure. For example, Zr changes from hexagonal close packed to cubic body centered lattice because the thermal energies cause one electron to drop from the s+p shell to the 4d subgroup. Ti and Hf in the same column show the same allotropic transformation. Since heat causes a metal to expand and the electronic structure to change (allotropic transformations), an applied stress can cause the electronic structure to change. The difference in shell size between outer (s+p) electrons and inner d-electrons should be expected to cause electronic movements between these shells due to stress or compression. As illustrated in Figures 6, 7, and 8, the interatomic distances of Cr, Mo, and W are rather close to the lower curves which relate to pure d electron bonding; whereas the atomic distance of K, Rb, and Cs are on the upper curves which relate to pure s electron bonding. In the extreme cases where the actual interatomic distances are either close to the lower curve or upper curve, the electron movements between the outer

shell and the inner shell are much less likely to happen because of the big promotion energy between two shells. If the interatomic distances of these elements are located between the upper and the lower curves where the promotion energy between two shells is the smallest, the largest electron movements should be expected. In general, electron movements between the outer shell and the inner shell are dependent on the promotion energy between the two shells and the bonding energy. Therefore, a greater tendency for electron movements under stress should be expected in Ti, Zr, and Hf which are placed in a region of smaller promotion energy than that of Cr, Mo, and W where the atomic size changes little with increasing electron concentration.

The electron movements between the outer shell and the inner shell associated with stress may be determined in an adiabatic heat experiment. The internal energy change of the elements due to stress can be calculated from the heat created by the stress minus the input mechanical work. The internal energy change is considered to be due to electron transfer between the outer shell and inner shell in the metals. Then, by comparing the promotion energies between the different energy levels, the tendencies of the electron movements could be determined.

CHAPTER III

EXPERIMENTAL APPROACH

The purpose of the experiment is to find the indication of the electron movements between the outer shell and the inner shell in metals associated with tension. As described in the preceding chapter, the electron transfers are indicated in the adiabatic heat under stress.

In order to obtain the adiabatic condition, the application of a cyclic stress was chosen as the method of applying a stress. The frequency of cyclic stressing should be high enough to prevent heat from exchanging with the surroundings, but slow enough to be easily recorded. Such a requirement of the dynamical process was achieved by employing a punch press machine with frequency of four cycles per second, combined with a loading spring. The photographs and the sketch of the arrangement of the punch press machine, loading spring, specimen holder and specimen are shown in Figures 9-12, respectively.

As shown in Figure 12, the loading spring consists of two pieces of spring steel ($3\frac{1}{2}$ feet long, 3 inches wide, and $\frac{1}{4}$ inch thick) assembled with two ball bearings at each end for the purpose of preventing friction at the joint. The loading spring which served as main part of the cyclic loading system was connected to the punch press machine at one side and the specimen at the other. As the head of the punch press machine, P, moves up and down cyclically, the spring is loaded and unloaded whereby a cyclic load is applied to the specimen.

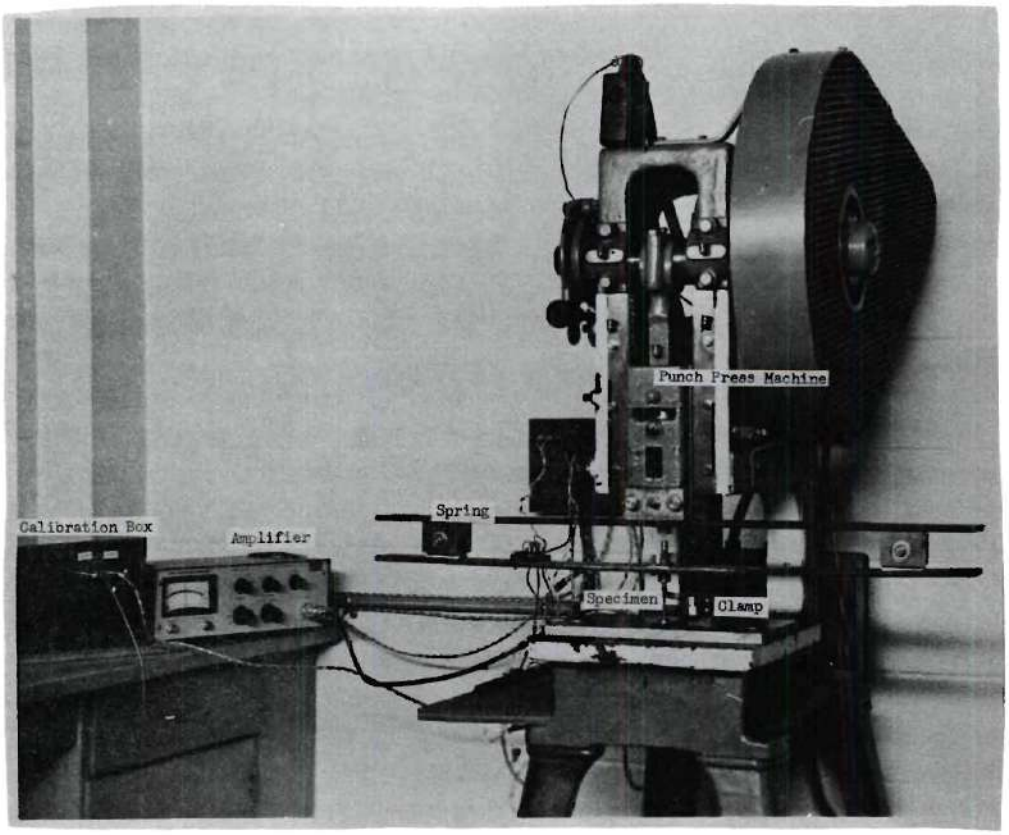

Figure 9. Arrangements of Punch Press Machine, Amplifier, and Temperature Calibration Box.
(A refers to amplifier, T refers to temperature calibration box.)

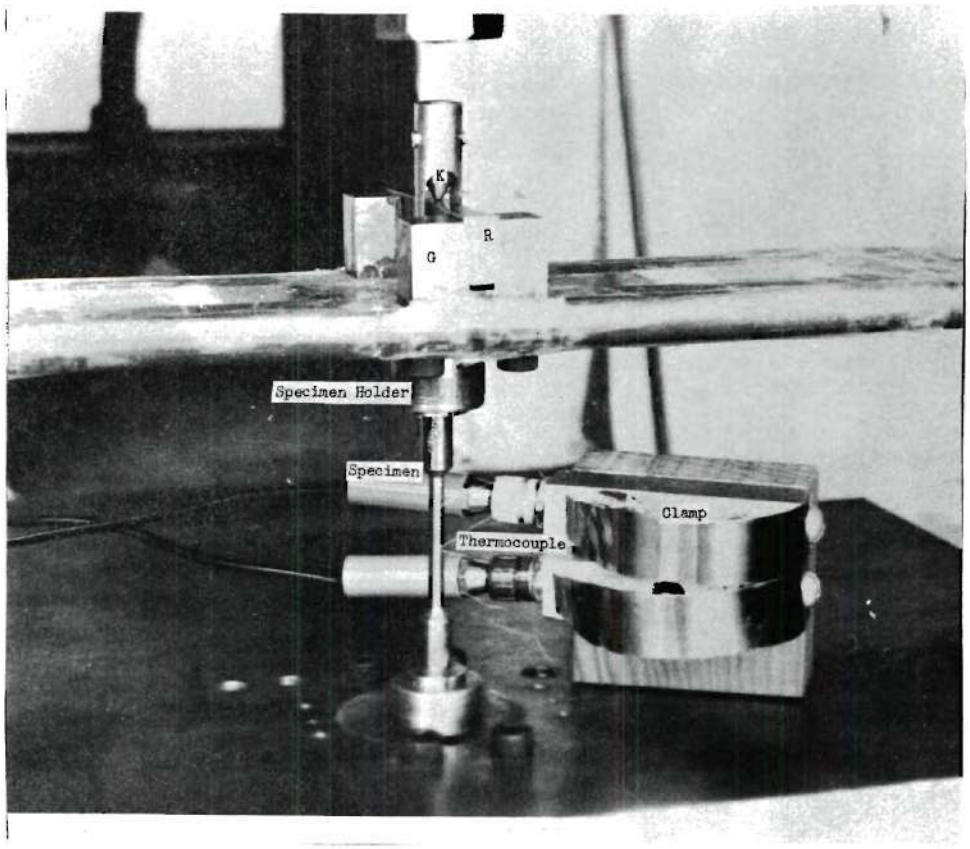

Figure 10. Arrangements of Specimen Holder, Specimen, and Clamp

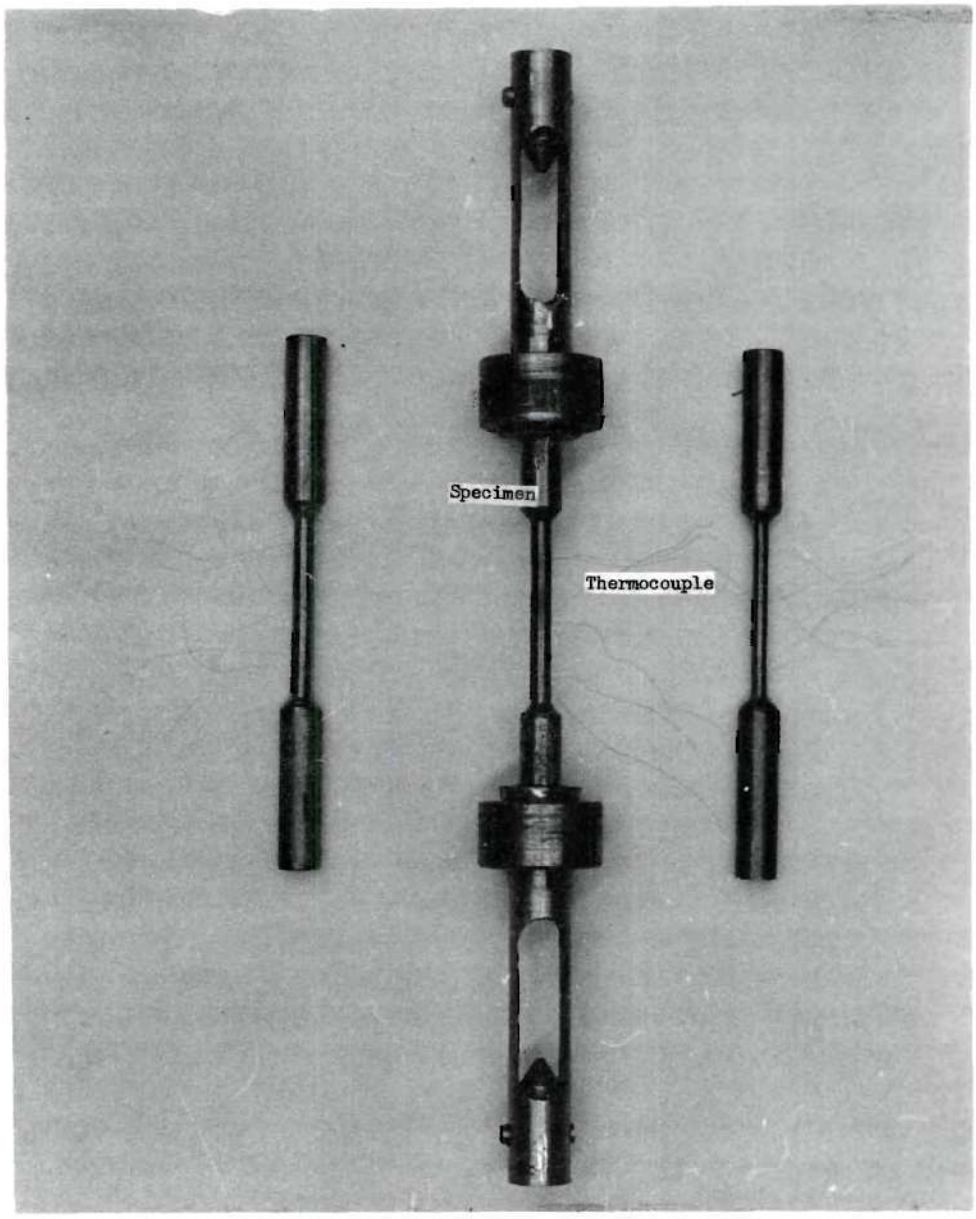

Figure 11. Detail of Specimen and Specimen Holder

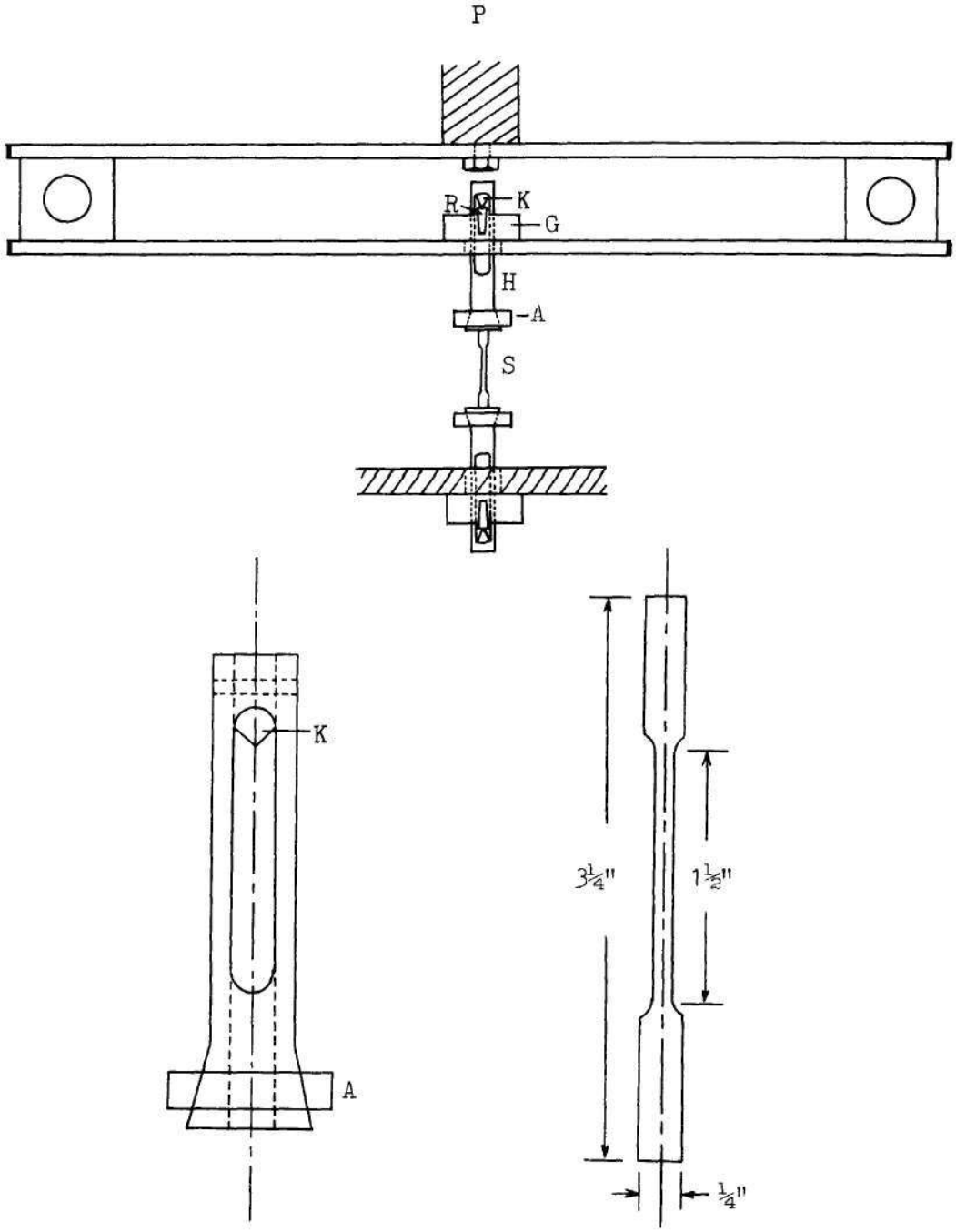

Figure 12. Schematic Diagram of Spring, Specimen Holder, and Specimen

As shown in Figure 11, the specimen, S, was a tensile test specimen consisting of a one and one-half inch gauge length and two heads for gripping. Both ends of the specimen were fastened in specimen holders, H, by friction through a self-locking ring, A.

The temperature change along the longitudinal direction of the specimen associated with stressing will not be the same if the stress distribution on the specimen along the longitudinal direction is not uniform. In our experiments, the pure tension on the specimens is assumed. In other words, there must not be any bending moment on the specimen along the longitudinal direction. In order to achieve pure tension on the specimen, the connection between the specimen holders and the loading spring or the base of the punch press machine was made by a special system of links, the details of which are included in Figure 12. The specimen holders were supported by the sharp point, K, on the rods, R, which were removable from the groove, G, on the spring or base of machine because of the convenience of specimen mounting. This link permitted the specimen to align itself so that the state of stress approached pure tension and the bending moment, due to alignment, was minimized.

In order to check the stress distribution, three pairs of thermocouples were welded to the surface of the specimen along the longitudinal direction. If there were a nonuniform stress distribution on the specimen, the corresponding temperature variation of three different pairs of thermocouples would show the different results. The alignment of all specimen tested in these experiments was checked by means of getting the same results from three pairs of thermocouples.

CHAPTER IV

INSTRUMENTATION AND CALIBRATION

Instrument Arrangements

The block diagram of instrument arrangements is shown in Figure 13. The temperature variations were measured by means of thermocouples. The signals from thermocouples were amplified and recorded by a visicorder. The load was measured with strain gauges and recorded by another channel on the same visicorder. Four strain gauges mounted on the loading spring were connected to make a Wheatstone bridge for load variation measurement. The potential changes from the Wheatstone bridge due to load variation was directly recorded on the visicorder. Since the temperature variation due to stressing was too small to record directly, an amplifier was employed before recording on the visicorder. Both temperature and load variations were recorded simultaneously on light sensitive photographic paper. In addition, a precision potentiometer was used for standardizing the power supply for the Wheatstone bridge on the spring and for calibration of the temperature system.

Instruments

The temperature and load variations were recorded by a Honeywell Model 1508 Visicorder, which was a rack mounted direct writing oscillograph, as shown in Figure 14. Recording frequency ranges from zero to 5000 cycles per second, depending on the type of galvanometer used. In

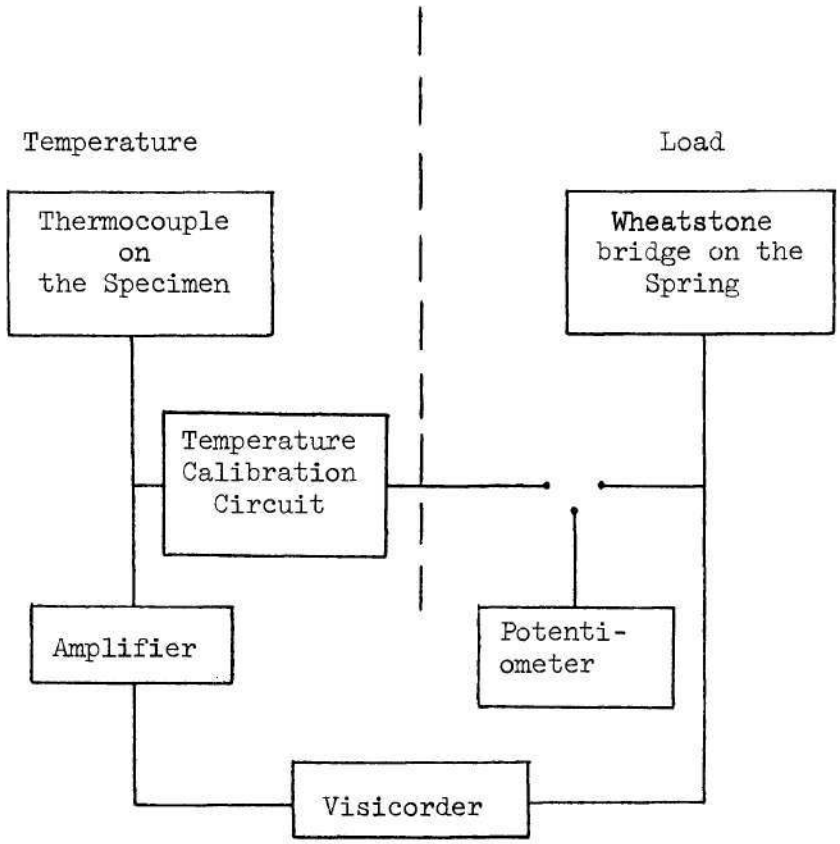

Figure 13. Block Diagram of the Instrument Arrangements

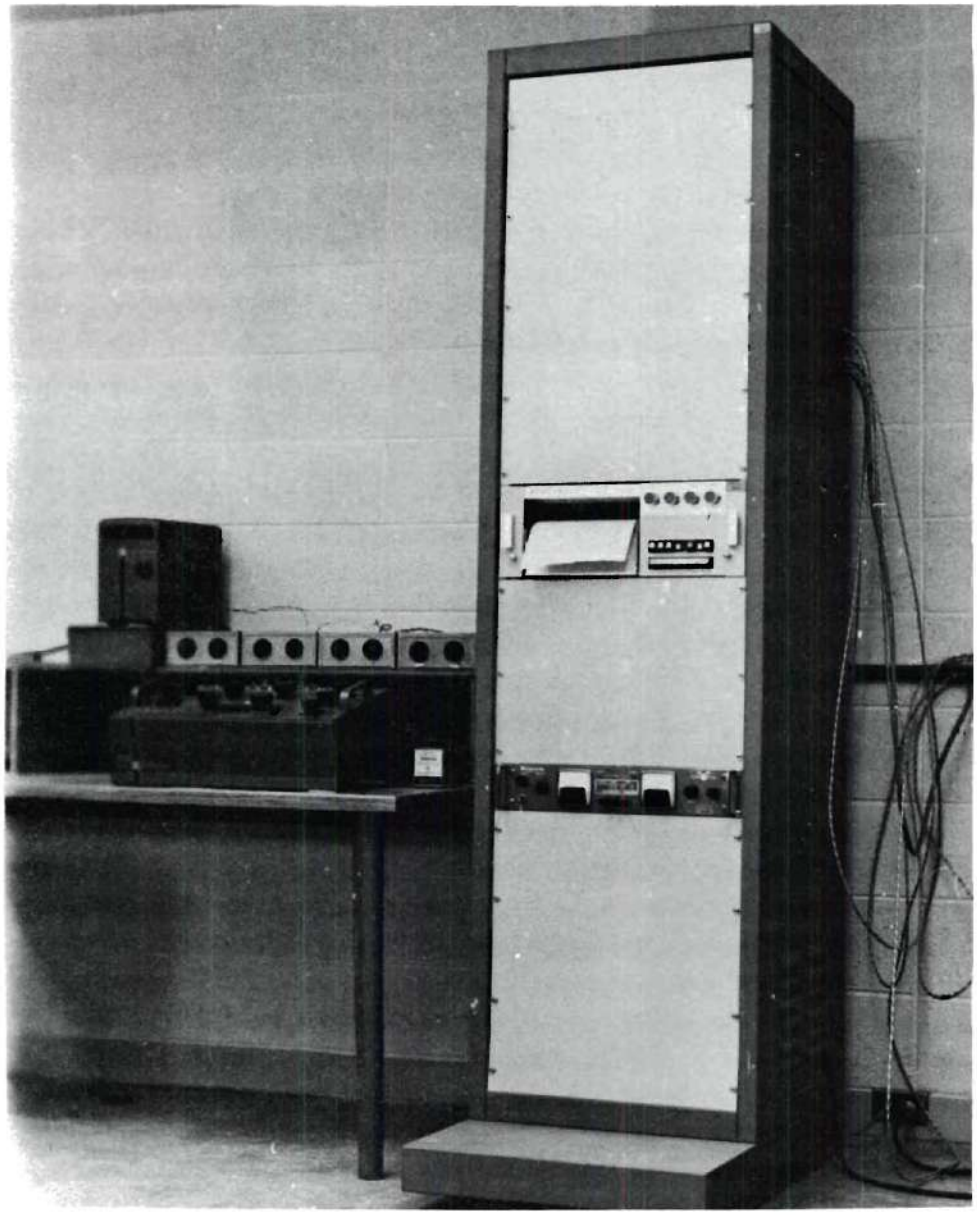

Figure 14. Visicorder and Potentiometer

our case, the electromagnetic damped galvanometers were used, M40-350A galvanometer for temperature measurement, M100-350 galvanometer for stress measurement. The flat frequency response and voltage sensitivity of galvanometer M40-350A and M100-350 were 0-24 cps, 0-60 cps, and 0.250 mv/in, 0.432 mv/in, respectively.

Because of the small thermal electromotive force measured, a Keithley Model 148 Nanovoltmeter was used as the amplifier before recording on the visicorder, as shown in Figure 9. Noise is negligible for the 0.03 millivolt range. Another advantage is that it can be operated by battery, permitting complete isolation from a power line, thereby eliminating many grounding problems. Since there is a chopper and input transformer in the amplifier, the time lag and the low frequency overshoot should be taken into consideration. The approximate magnitude of overshoot was around 1.7 percent for all ranges. Detailed calculations of overshoot for different amplification ranges are presented in Appendix I.

Owing to maintenance of the constant D.C. source on the strain gauge and temperature calibration circuit, a precision potentiometer was required. In our experiment, Leeds Northrup 7553 Type K-3 Universal Potentiometer was used for this purpose, as shown in Figure 14. The measuring range goes from zero to 1.6110 volts.

Temperature Measurement and Calibration

The specimen was surrounded by a sleeve of soft insulation mounted on a metal screen to protect it from the influence of heat from convect-

ing air. The specimen temperature variations were measured by a thermocouple made by spot welding two thermocouple wires to the surface of the specimen in the longitudinal direction. Elements with high thermal conductivity, such as Ag, Au, and Cu, could not be welded on and the thermocouple wires were pinched on. A chromel-constantan thermocouple was used because it gave the largest electromotive force of any of the generally available couples. Because of the effect of thickness of thermocouple wire on the response time of measurement, the thinner wire is desirable for quick measurement. In our case, the two mil diameter wires were chosen. However, the temperature effect associated with stress is still too small, usually in the range of microvolts, to be recorded directly by the visicorder, so that the Keithley nanovoltmeter was used with an amplification gain of about one thousand times.

In measuring small potentials in this experiment, the thermal noise becomes extremely significant. Electrically shielded copper cable and clamps therefore were used for the connection between the specimen thermocouple and the amplifier.

Owing to the temperature variation of one tenth of a degree centigrade, the conventional temperature difference calibration methods failed to meet our experimental requirements. Therefore, a special electrical calibration circuit was built for this purpose, as illustrated in Figure 15. In this circuit, a series of one 260,000 ohm and four standard one ohm resistors was connected to a D.C. source. Four one ohm resistors in series were connected to a five step switch. The potential between AB could be measured accurately to fourth decimal by the Leeds &

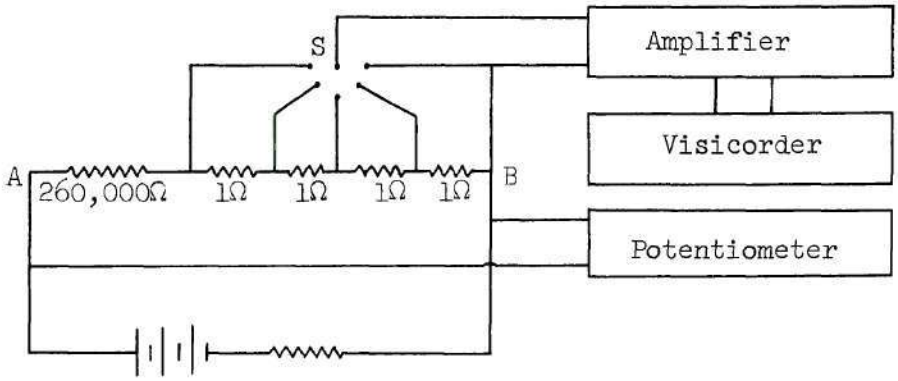

Figure 15. Electric Circuit of Temperature Calibration

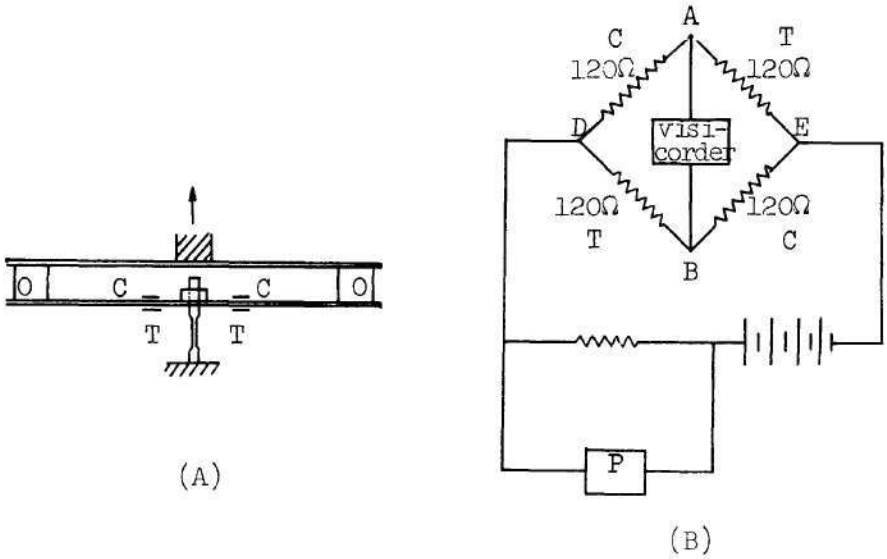

Figure 17. Wheatstone Bridge of Strain Gauge on the Spring
(C refers to compression, T refers to tension)

Northrup potentiometer. In this way, the accurate potential between each step and the ratio of deflections on the visicorder to known potentials could be observed easily. The details of calculation and data will be reserved for Appendix II. The typical curve of temperature calibration is demonstrated in Figure 16, in which each step corresponds to about four microvolts.

Load Measurement and Calibration

The load system consisted of the loading spring connected to the punch press machine. The load could be varied from zero to 125 kg with a frequency of four cycles per second. The specimen was mounted under slight tension to keep it in place while loading was not applied.

In order to measure the load variations, a strain gauge Wheatstone bridge circuit was employed, as shown in Figure 17. Four identical resistance strain gauges were glued on the fine ground surface of the lower spring; two were on the top side and two were on the bottom side of the spring. As illustrated in Figure 17, the top side of the lower spring was under compression and the bottom side was in the tension when the spring was pulled upward, that is under load position. The strain gauges were arranged as in Figure 17(B) so as to gain the greatest potential difference between A and B, which was recorded on the Honeywell Photographic Visicorder directly. The constant D.C. supply on the terminal DE was standardized by Leeds & Northrup potentiometer before and after each experiment.

The calibration of the load in kilogram force to corresponding

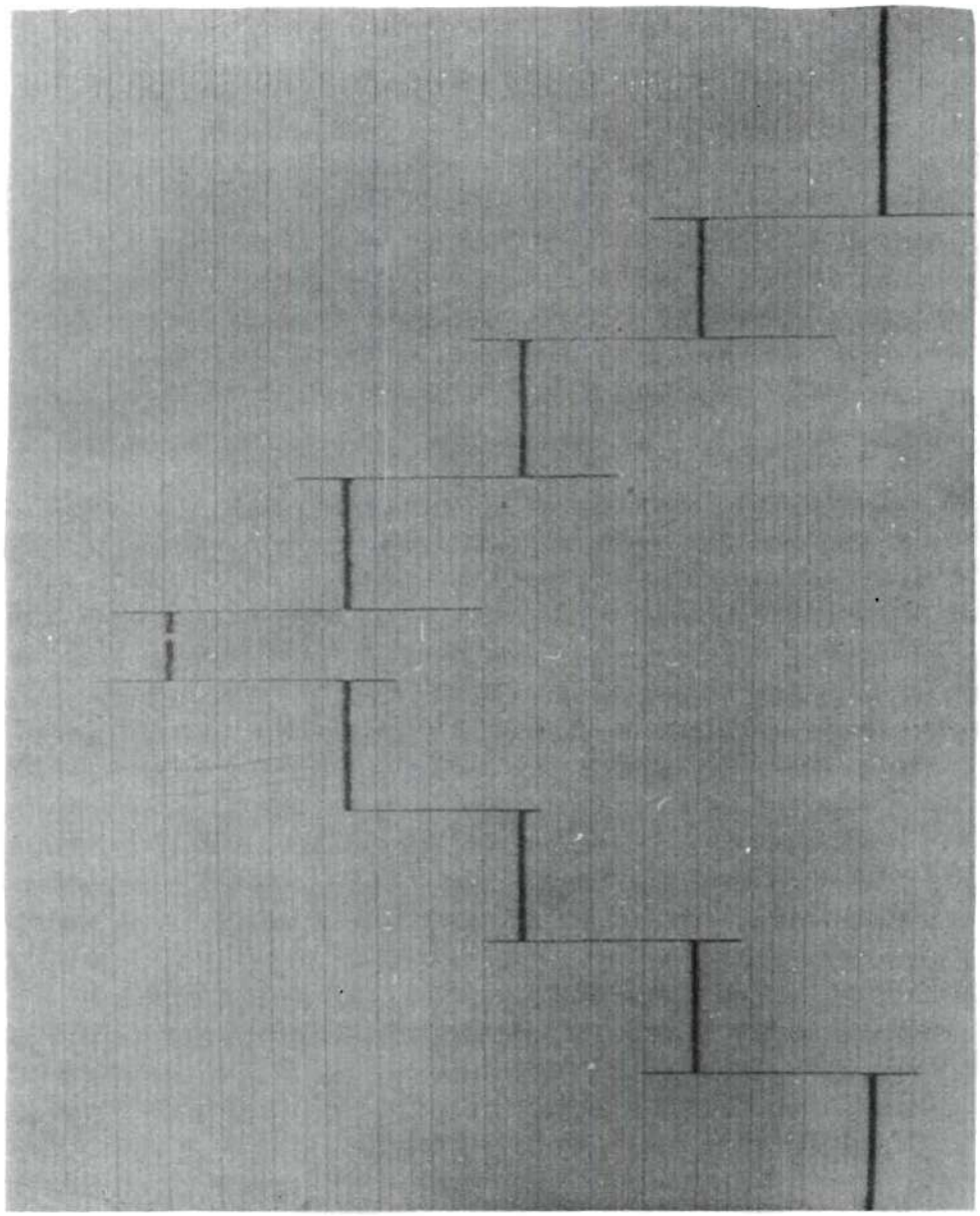

Figure 16. Typical Curve of Temperature Calibration (The overshooting is due to short circuit of amplifier input while switching the steps.)

deflection on the visicorder was done by hanging calibrated weights on the spring. The typical curve of load calibration is shown in Figure 18. The numerical data were listed in Table 1 and the plot of load versus deflection on the visicorder is shown as a straight line in Figure 19. Therefore, the deflection on the visicorder was a linear function of load. In other words, the spring is within the elastic range below 130 kg load. This will simplify the calculation of the results.

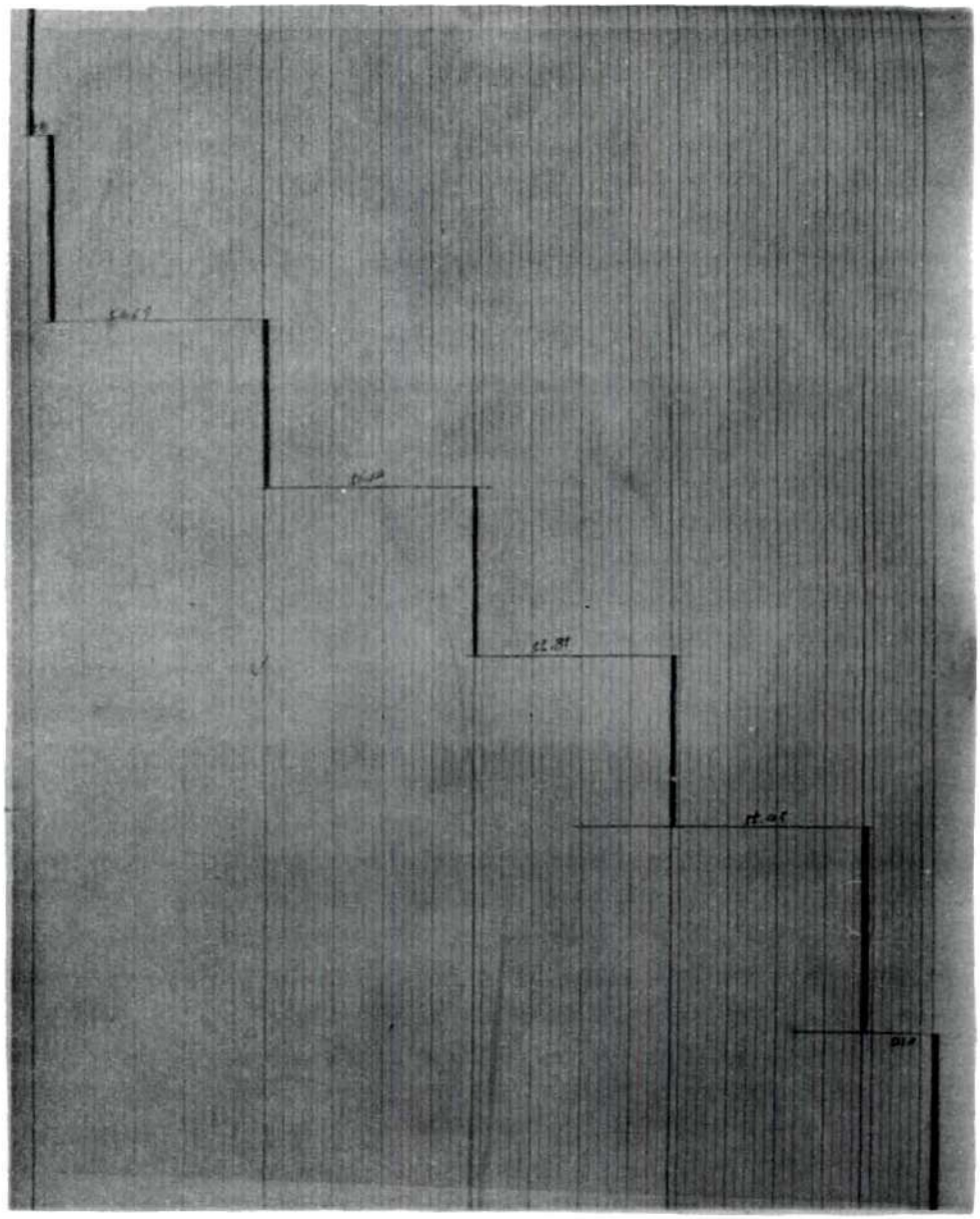

Figure 18. Typical Curve of Load Calibration

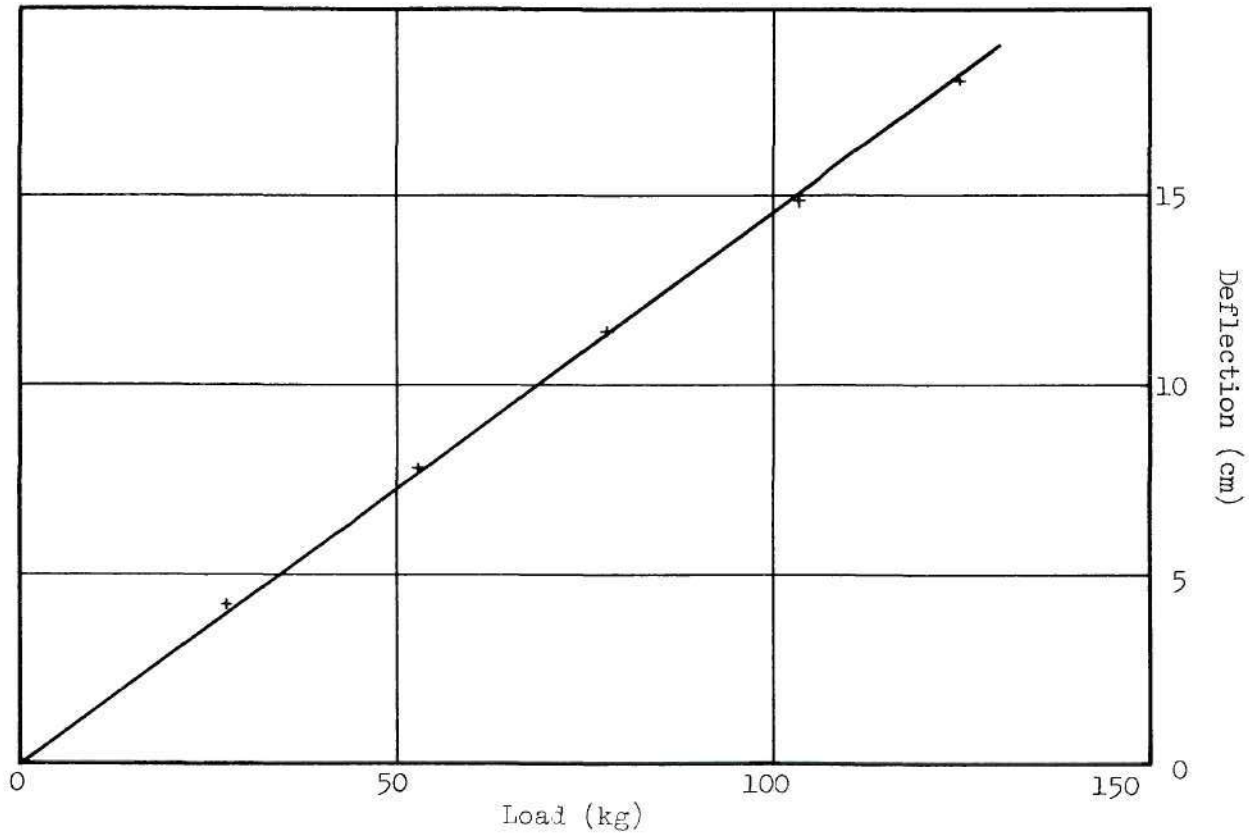

Figure 19. Plot of Load on the Spring versus Deflection on the Recorder

CHAPTER V

DISCUSSION AND RESULTS

Specimen Preparation

The majority of the specimens were made of one-fourth inch diameter rods except in some special cases due to the limitation of the yield strength and materials cost, in which cases three-sixteenths inch and one-eighth inch diameter rods were used. The gauge length of the specimens was turned down to the desired diameter on a lathe. Since the maximum load was constant, the stress level on the specimen was controlled by variation of the diameter.

Several factors in the preparation of specimens were carefully studied. First, the influence of deformation was studied by comparing the temperature increases of a cold worked specimen with an annealed specimen of the same material. For this purpose a titanium specimen was encapsulated in inert gas in order to prevent oxidation during heat treatment and annealed at 1200°F for half an hour. The temperature rise of this specimen was compared to the cold worked specimen. The hardness of the specimens was R_B 99.5 before and R_B 81 after anneal under the load 100 kg. In fact, deformed and annealed materials showed the same effect. Iron and copper received the same experimental treatment and showed that there was no influence of cold work on the results when hardness was reduced from R_B 80 to R_B 37 and from R_B 85 to R_B 45, respectively. As a consequence of these experiments, specimen prepara-

tion could be simplified since cold worked materials could be used. This result permits the use of higher stresses yielding larger signals and the greater accuracy could be obtained.

Second, the influence of different stress levels on the temperature variation was studied. A group of specimens of the same material with different diameters was prepared for this purpose. Since the ratio of temperature variation to stress for different specimens was found to be constant, no special caution had to be taken in order to work with fixed predetermined stresses. Therefore the diameter of the gauge length of the specimen was chosen to yield a stress as close to below the yield strength as possible. The yield strength of different materials and the chosen diameters are listed in Table 2.

Accuracy of Measurement

The errors in these experiments can be divided into two parts; one is the systematic error and the other is the random error.

Systematic Error

According to the calibration data of the loading spring listed in Table 1, the average ratio of load in kilograms to the deflection in centimeters on the recording paper is 6.828 kg/cm. The calibration curve shows that the deviation of the loading spring from linear elasticity is ± 0.11 kg/cm. In other words, there is ± 1.5 percent error of the maximum loads, 122 kg, of the loading spring corresponding to 17.6 cm on the recording paper in our measurement. The magnitude of this error is acceptable for our experiment.

As mentioned in Chapter IV, the noise is negligible for the 0.03

millivolt range and the error due to the low frequency overshoot of the amplifier is 1.7 percent for all ranges. The whole error of temperature measurement will therefore be about 1.7 percent. Considering the technical difficulties in measuring such small temperature changes, the quality of our temperature measurement is acceptable since the whole systematic error on evaluation of both load and temperature did not exceed 3.2 percent.

Random Error

The stress distribution within the specimen along the longitudinal direction is occasionally not completely uniform due to the nonuniform diameter or non-central loading of the specimen. Therefore a little scatter in the temperature measurement on three pairs of thermocouples along the longitudinal direction was occasionally observed. The magnitude of such random errors is different from specimen to specimen and depends on the quality of the machining and the mounting of the specimen in the holder. Usually such deviations are within ± 2 percent. In addition, the heat of spot welding the thermocouples on the specimen surface could cause a local grain size change and an oxidation, and could be another reason for getting different thermocouple readings on three pairs of thermocouples. In order to study the influence of the oxidation on the temperature measurement, the comparison between welding the thermocouples on polished and oxidized aluminum specimen surfaces was made. In addition, the influence of pinched thermocouples on the temperature measurement was also studied. It showed that there were little differences of the temperature variations among the three different

surface conditions. Actually the surface of the specimen was polished before making the spot welding for every specimen. The scattering of temperature measurement due to oxidation of spot welding was not taken into account in these experiments.

In order to measure the temperature as correctly as possible, the experiment was kept close to ideal adiabatic conditions. For this purpose the experiments were run cyclically with a reasonably high frequency and the continuous sinusoidinal curves of temperature and load were recorded simultaneously, as shown in Figure 20. The width of the deflection of temperature was measured between the two parallel lines which were drawn across the peaks of several cycles. In this way, the average value of the deflection of temperature was obtained graphically. The random errors due to the scattering of temperature measurement around the average value were dependent on different elements. In addition, the line thickness on the recording paper, one millimeter wide, also affected the accuracy of evaluation of curves. To avoid line thickness error, measurements were always taken from the same side of the line. Generally speaking, the greater deflection of the curves, the less the random error. The same amount of random error in 10 cm deflection, such as one percent, will cause twice the random error in a five centimeter deflection. That is the reason why the experiment should be run at the highest stress level possible.

Random error comes from slight bents in the specimens (two percent), thermocouple errors (one percent), and graph reading errors (one percent), which total four percent. Be repeated readings of three thermocouples, the random error actually became smaller than indicated.

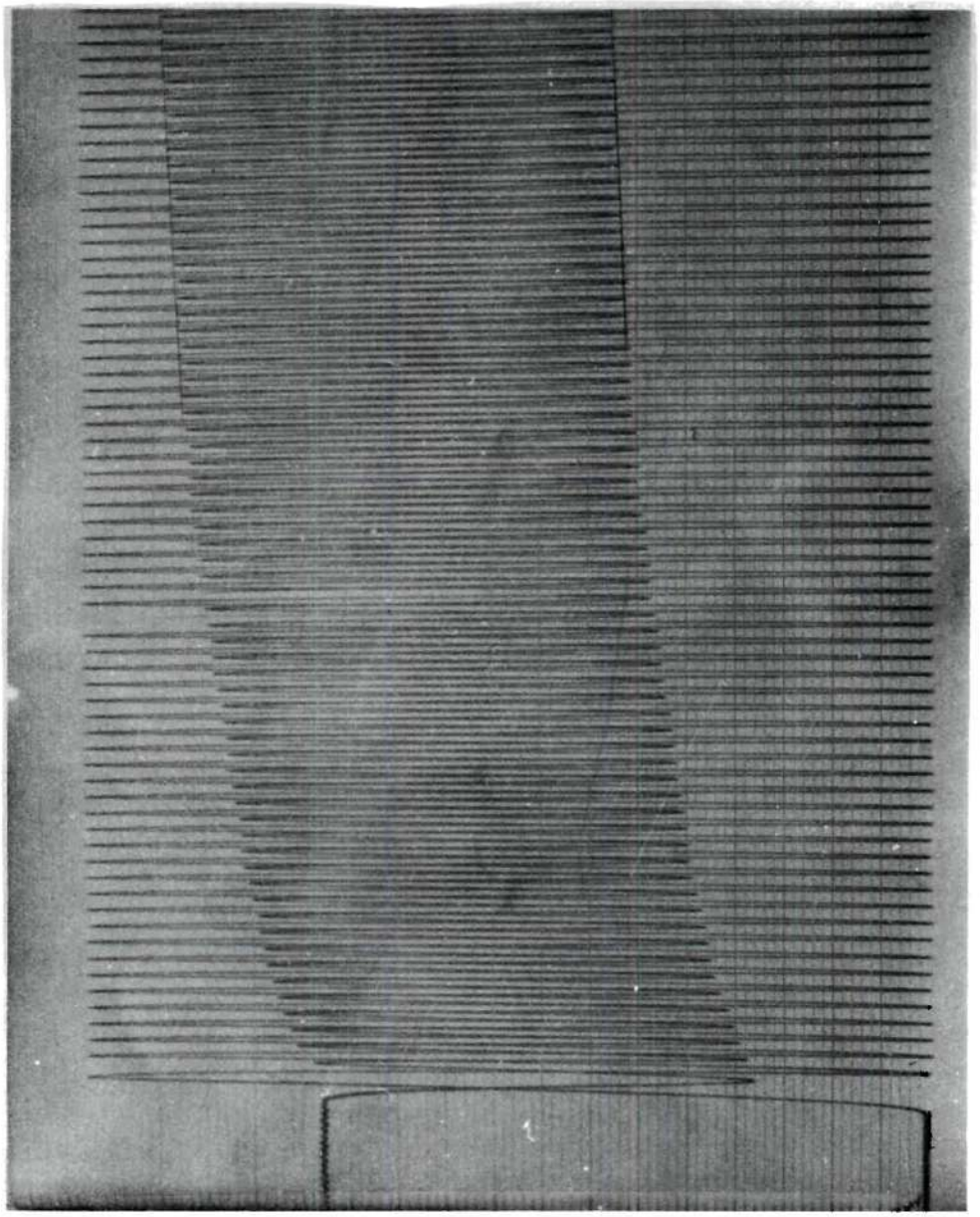

Figure 20. Typical Curve of Temperature and Stress

Systematic error and random error together did not exceed seven percent. The quality of our measurement data is within acceptable accuracy and is sufficiently reliable for future analysis.

These experiments were assumed to be run under adiabatic conditions. The approach to the adiabatic condition was studied by checking the temperature stability in a single cycle. If the frequency of stressing is not high, the temperature curve will have a chance to drift after each cycle. If the experiment was carried out under adiabatic conditions, the temperature curve will remain stable after a single cycle. As shown in Figure 21(A), the temperature curve of Cu remained constant before and after one cycle. Therefore this experiment can be assumed to have run in the adiabatic condition. The elements with good thermal conductivity, such as Ag, Au, and Al, were checked in a similar manner. Since heat exchange essentially will be by thermal conduction through the ends of the specimen, materials with lower thermal conductivity will be close to ideal adiabatic condition. In a similar manner, the ideal adiabatic conditions were checked by a half cycle operation. As shown in Figure 21(B), the temperature curve remained constant before and after a half cycle. This shows that the experimental conditions are very satisfactory.

Experimental Results

In the present experiments, temperature and load changes are recorded simultaneously, as shown in Figure 18. The deviations of the temperature and load are chosen opposite for the purpose of clarity in presentation. The drifting of temperature in the first few cycles is

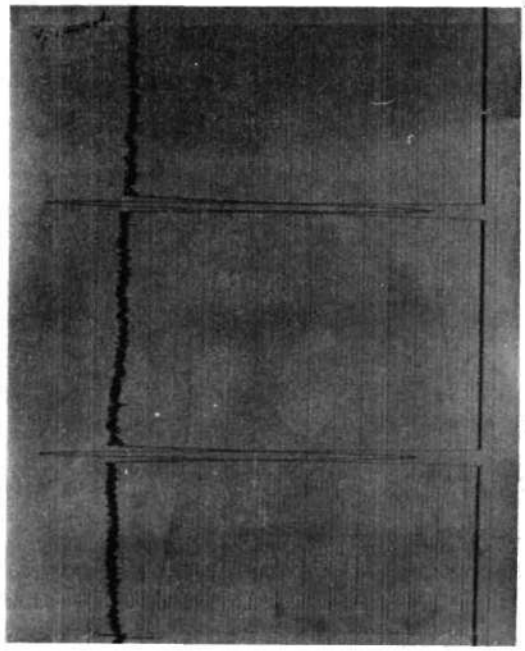

(A) Single Cycle

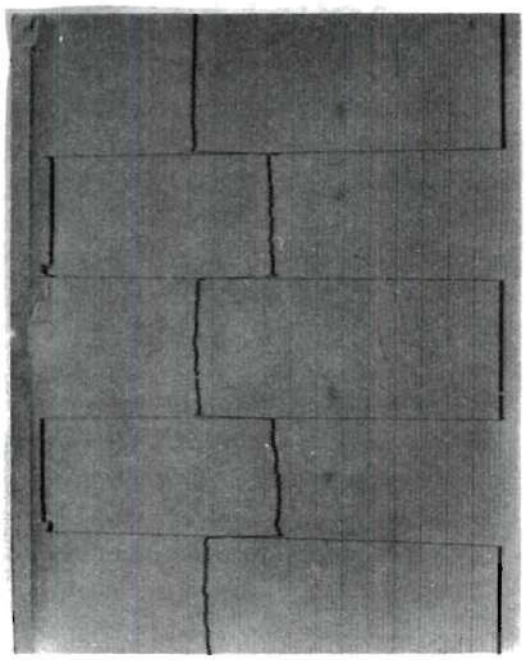

(B) Half Cycle

Figure 21. Typical Curve of Temperature and Stress with a Single Cycle and a Half Cycle

due to the internal friction (damping) which changes the temperature of the specimen. The tendency for the average temperature increase of these curves varies with the material. The temperature reaches equilibrium after the heat of internal friction is compensated by heat losses which occurs after a few cycles. The experimental temperature change was evaluated after reaching constant average specimen temperature.

The graphical deflections were converted to degree centigrade and kilogram by multiplying with the appropriate conversion factors. These conversion factors are described in Appendix II and Table 1. The ratio of temperature change to stress change was calculated and listed in Table 3.

The adiabatic elastic deformation of a body is accompanied by a change in temperature and is known as the thermoelastic effect. Under adiabatic conditions the temperature of a metal bar is decreased by an elastic elongation and is increased by an elastic compression. In the present investigation, only an elastic elongation applied. The relationship between the temperature and stress changes can be derived from thermodynamic arguments (18):

$$\frac{\Delta T_s}{\Delta \sigma_s} = - \frac{T \alpha_1 V_1}{c_p}$$

where α_1 is the coefficient of linear thermal expansion, V_1 is the atomic volume, and c_p is the specific heat. The sign of the temperature change ΔT is opposite to that of the change in stress.

The above equation was used to check the experimental data. The

calculated ratios of the change of temperature to stress of the fourth, fifth, and sixth period elements were listed and drawn in Table 3 and Figures 22 through 24, respectively. The values of the coefficient of linear thermal expansion, atomic volume, and specific heat in our calculations are listed in Table 4. In Figures 22 through 24, the dashed lines indicate the observed values and the solid lines represent calculated values. Comparing the observed values with calculated values in Table 3, we found that the observed values are larger than the calculated values in most of the elements except Zn. This systematic difference is very probably due to the instrumentation calibration. Since the linear coefficient of thermal expansion, the atomic volume, and the specific heat are involved in the thermoelastic equation, errors in these three quantities should be included in the calculated thermoelastic effect. The values of linear thermal expansion coefficient, however, are not particularly accurate. Therefore, the calculated values from the thermoelastic equation can only be expected to provide an approximate reference value for checking the experimental data. Considering the uncertain factors involved in the thermoelastic equation and the instrumentation errors, 10 percent difference between experimental and calculated values is satisfactory. It is, however, remarkable that the difference is constantly about 10 percent for the elements except Zn.

According to the thermoelastic equation, the temperature change is proportional to the change in stress. Thus the internal energy change can be calculated conveniently per unit stress or per unit strain

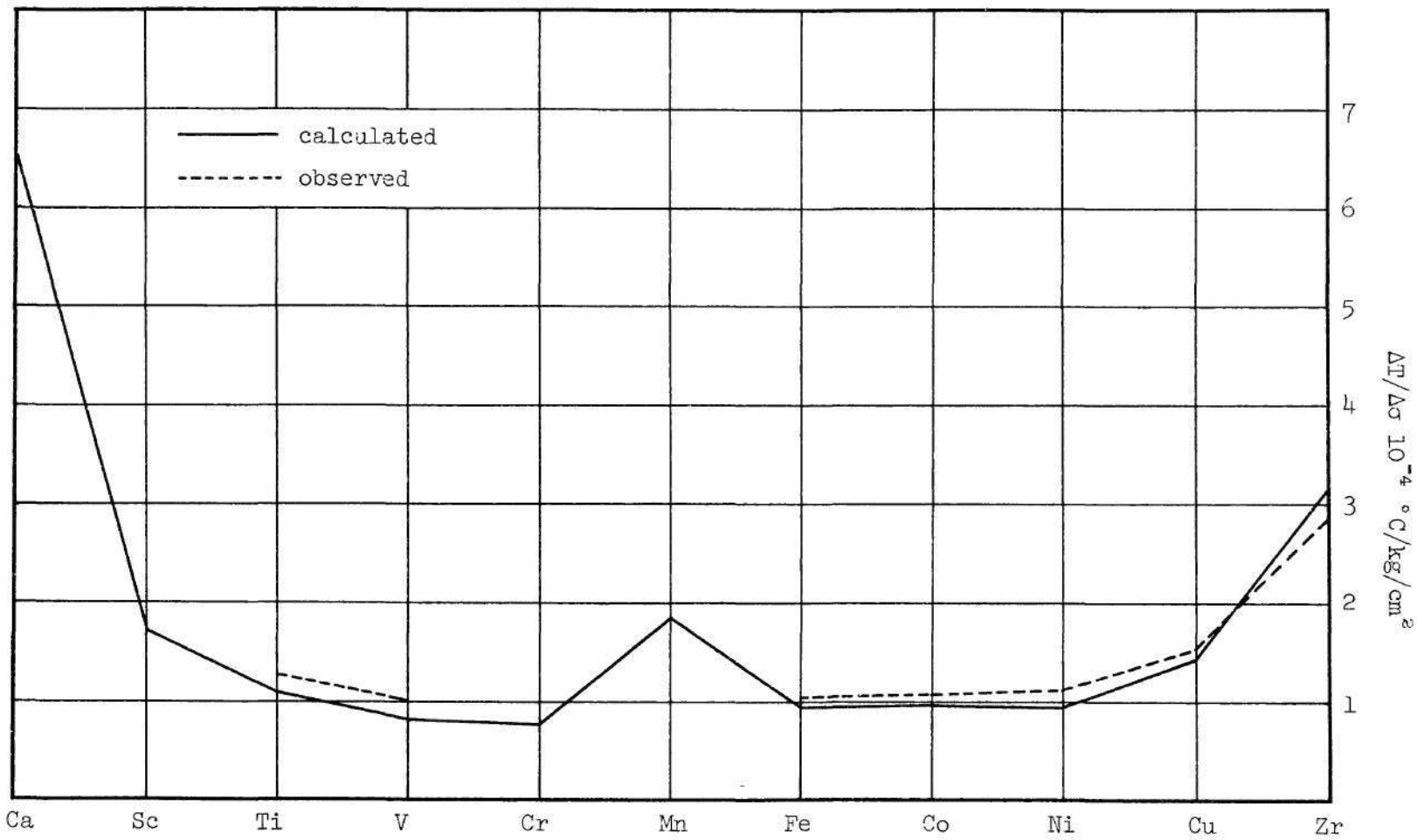

Figure 22. Comparison of the Calculated and Observed Value of $\Delta T/\Delta\sigma$ in the Fourth Period Elements

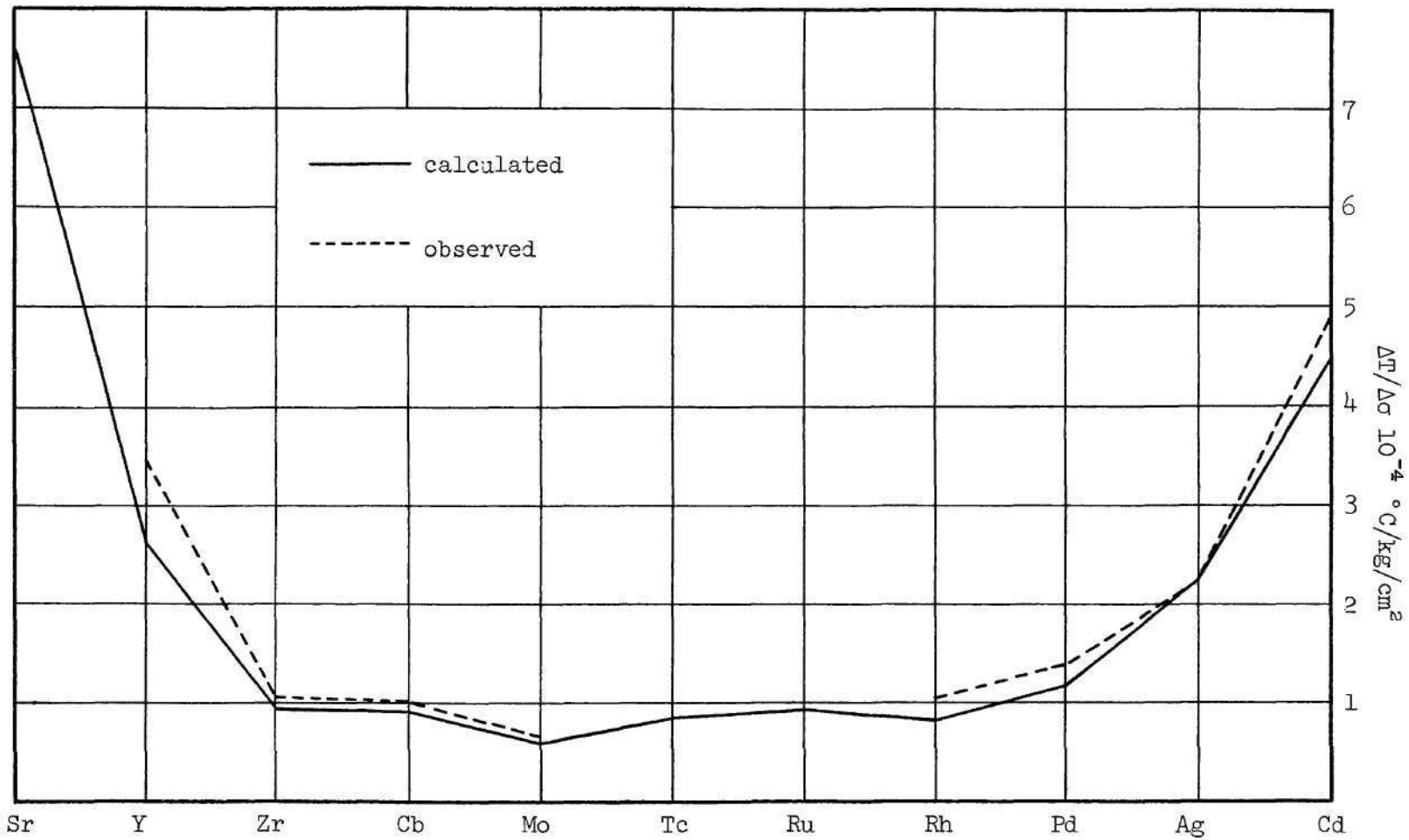

Figure 23. Comparison of the Calculated and Observed Value of $\Delta T/\Delta\sigma$ in the Fifth Period Element

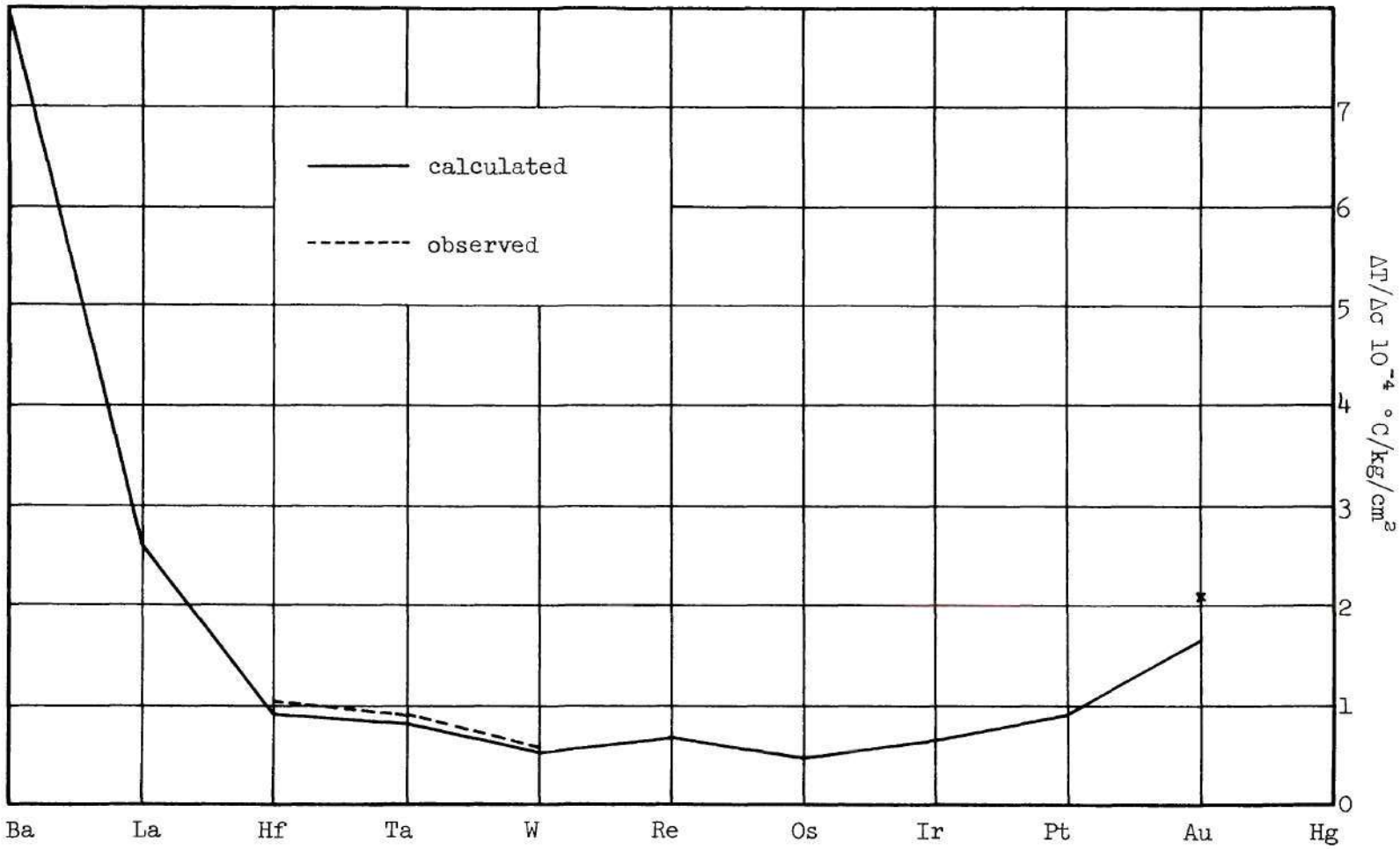

Figure 24. Comparison of the Calculated and Observed Value of $\Delta T/\Delta\sigma$ in the Sixth Period Elements

from the measured ratio of temperature change to stress change for each element. Such calculations are carried out for the purpose of easier comparison between elements over the periodic chart. The internal energy change can be calculated by subtracting the mechanical work done on the specimen from the heat change. The typical example of this calculation is given in Appendix III. The heat energy change ΔH, the mechanical work done on the specimen, and the internal energy change for the unit stress (1000 kg/cm^2) and the unit strain (0.1 percent) are listed in Table 5 and are plotted in Figures 25 through 27. Since the interatomic distance changes with stress are of interest, the internal energy change per unit strain will be compared with promotion energy.

Under adiabatic conditions, the temperature of a metal specimen is decreased by elastic elongation. In view of the atomic scale, the atoms vibrate about the lattice positions. The forces between the atoms are in equilibrium when no external forces are acting on the crystal. As an external force is applied, the equilibrium condition will be disturbed. In case of elastic elongation, the atomic distance will be longer in the direction of the applied force and the vibrational frequency of the atoms will increase. The vibrational energy of the atoms depends on the frequency. Therefore, increasing the frequency means absorption of energy which under adiabatic conditions is equivalent to a temperature drop. Therefore the influence of stress on atomic vibration change is one of the factors causing the internal energy change due to stressing. Because of the difficulties in calculating the atomic vibrational energy in solid state under stress, it will not be taken into

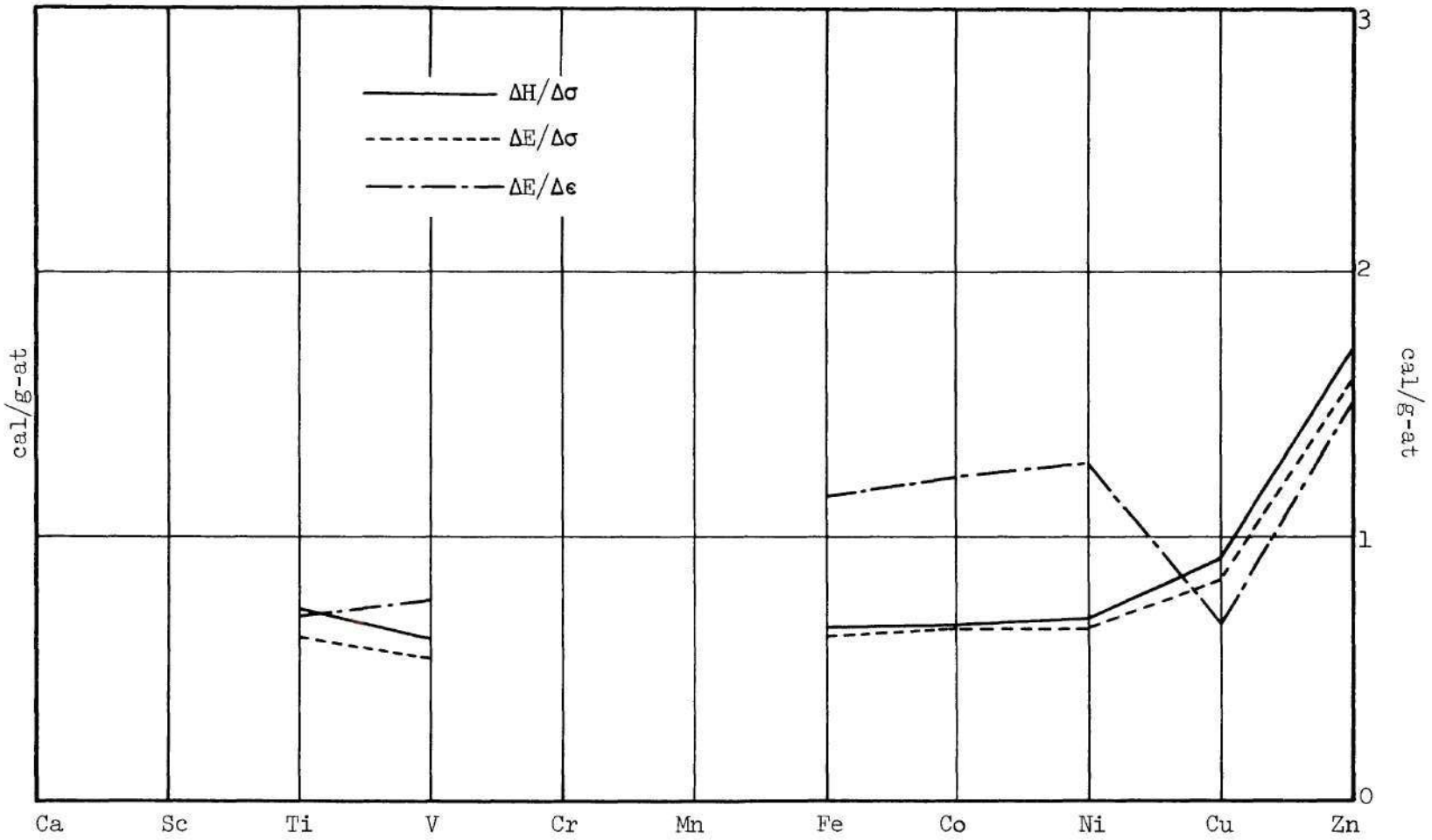

Figure 25. Change of Heat Energy and Internal Energy per Unit Stress and Unit Strain in the Fourth Period Elements

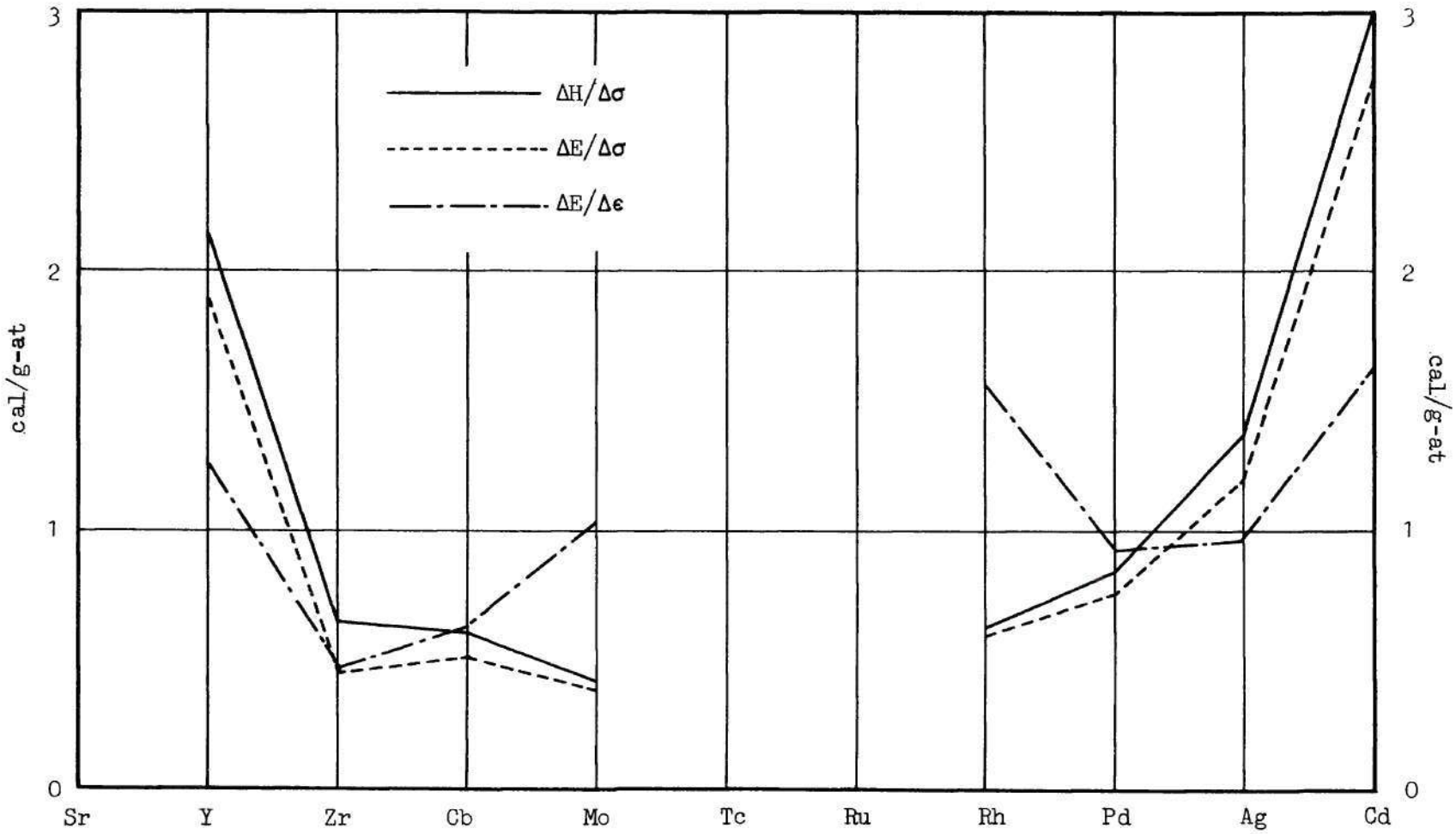

Figure 26. Change of Heat Energy and Internal Energy per Unit Stress and Unit Strain in the Fifth Period Elements

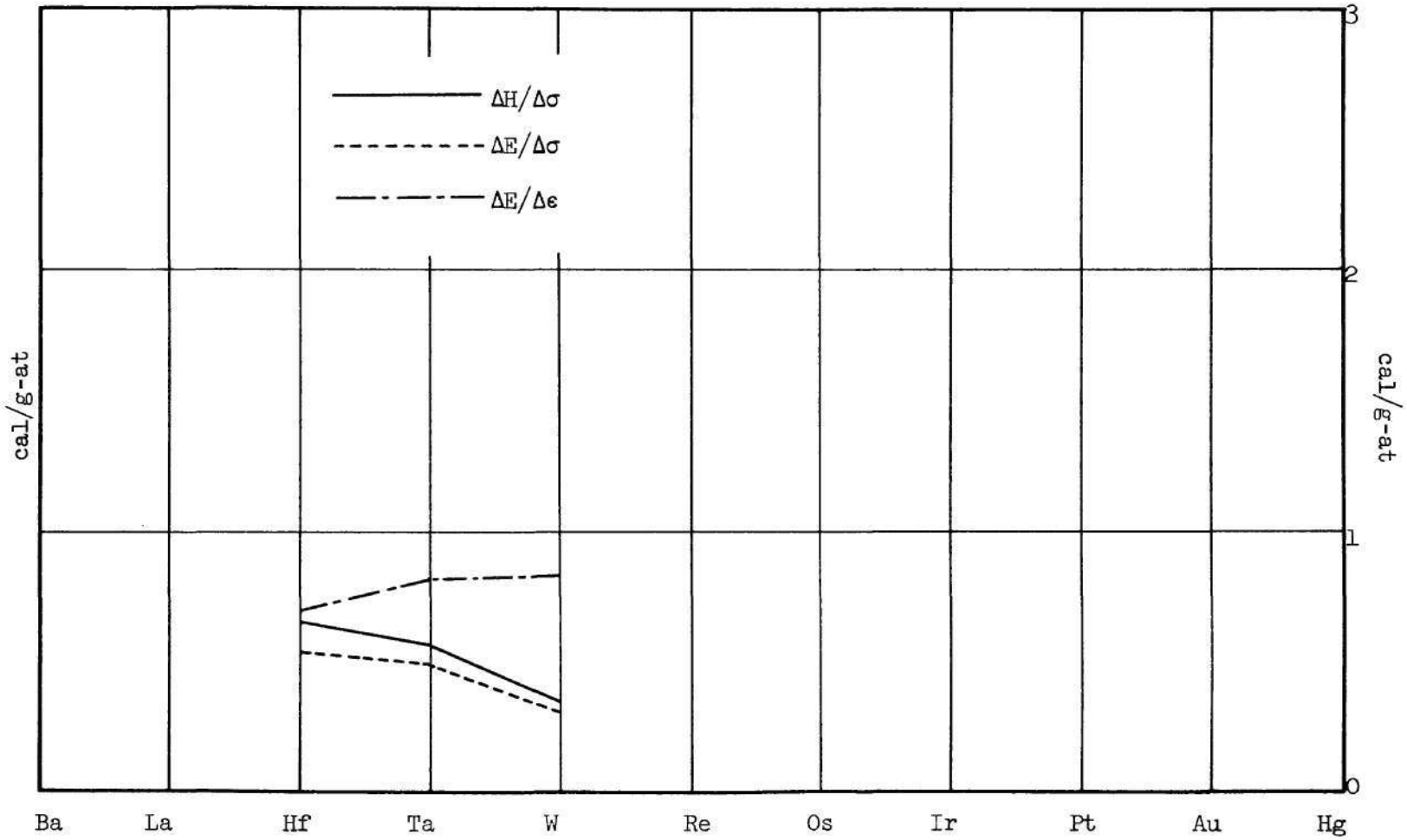

Figure 27. Change of Heat Energy and Internal Energy per Unit Stress and Unit Strain in the Sixth Period Elements

account until the data for internal energy change due to compression are available later on.

The other factor in the internal energy change due to stress is the electron transfer between the outer shell and the inner shell. According to Engel's electron bonding mechanism, the bonding electrons retain their specific character in the solid state the same as in free atoms. The spectroscopic data for the free atom could therefore be used for the analysis. By using spectroscopic data, the promotion energy for the electron configurations $d^{n-1}s$ and $d^{n-2}sp$ for the transition elements in the fourth, fifth, and sixth periods are listed in Tables 6 and 7. The relative promotion energy between $d^{n-1}s$ and $d^{n-2}sp$ for the fourth, fifth, and sixth periods are plotted as in Figures 28 through 30, respectively.

As illustrated in Figures 28, 29, and 30, the energies of each configuration are presented as bands because there are, in general, several spectroscopic states for each electronic configuration, corresponding to different combinations of the spin and orbital momenta of the electron. In general, the d orbitals, which are in an inner shell, become stabilized with respect to the s and p orbitals of the outer shell as the nuclear charge increases from left to right in a transition metal period. It can be seen that, for the first three metals, such as Ca, Sc, Ti, etc., in the three transition element periods, the two configurations lie close enough together in energy so that one might expect that the bcc ($d^{n-1}s$) and hcp ($d^{n-2}sp$) structures would be close together in energy. There is a great chance to cause an electron transfer

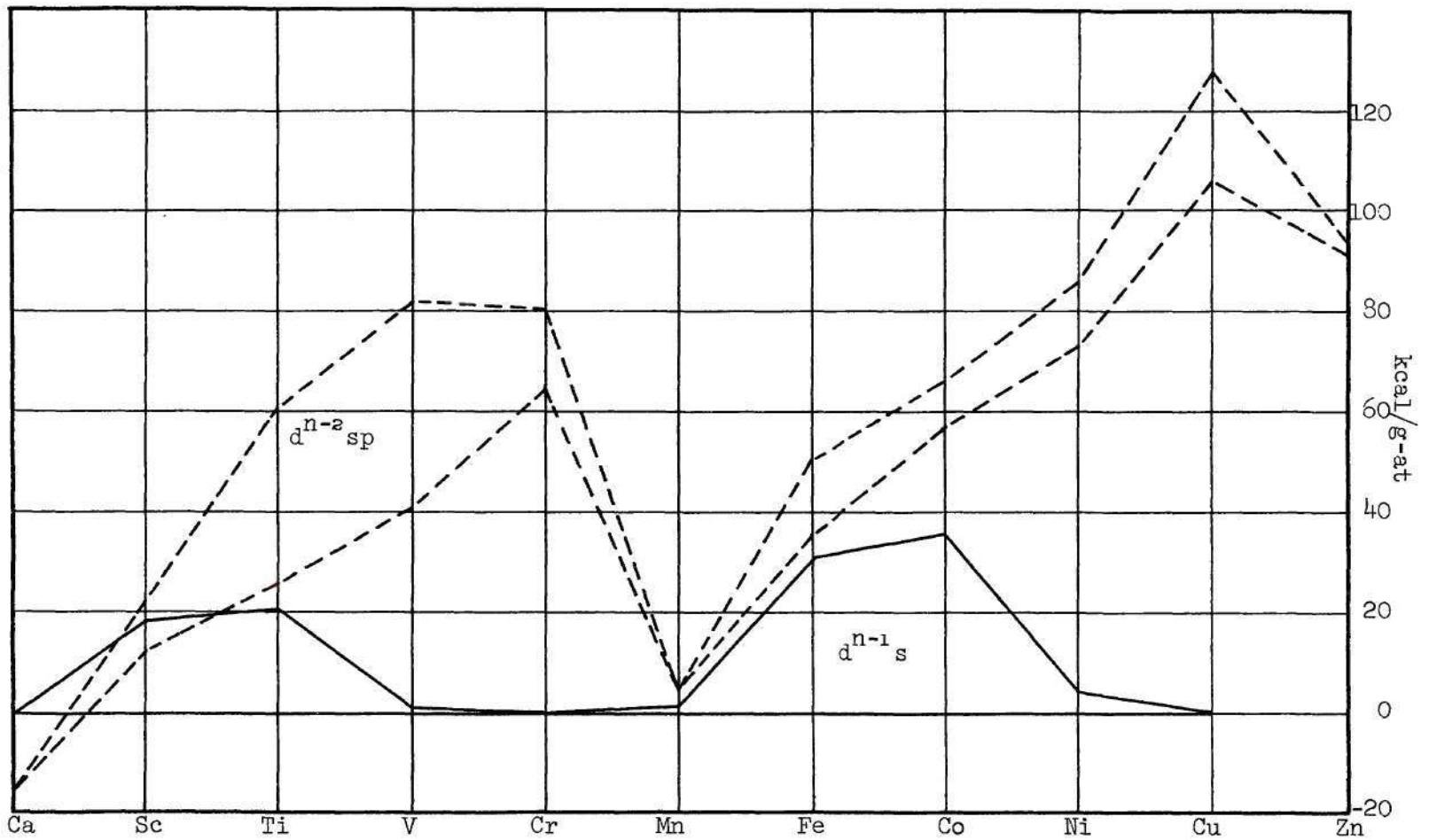

Figure 28. Relative Promotion Energy of $d^{n-1}s$ and $d^{n-2}sp$ Electronic Configurations for the Fourth Period Elements

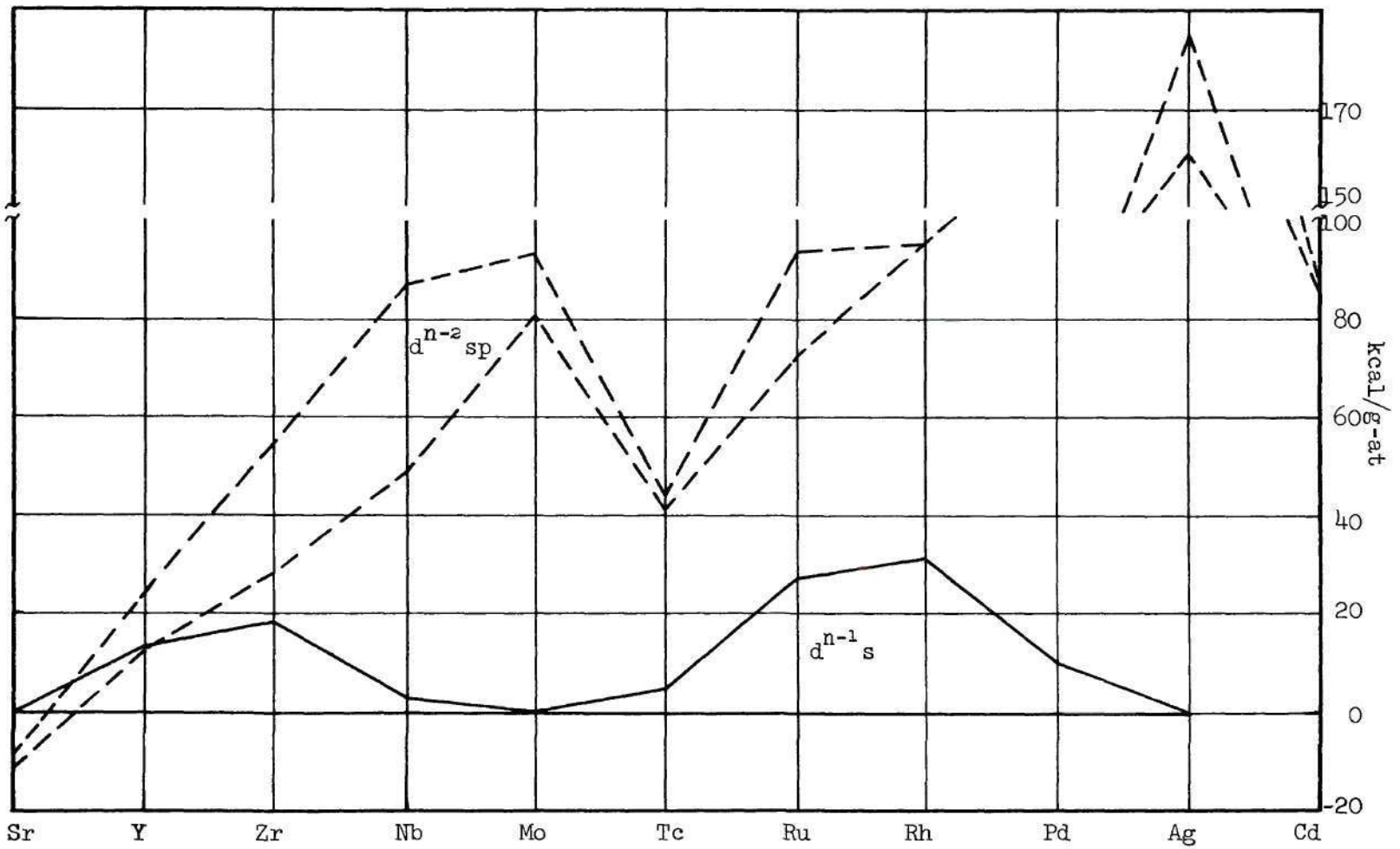

Figure 29. Relative Promotion Energy of $d^{n-1}s$ and $d^{n-2}sp$ Electronic Configurations for the Fifth Period Elements

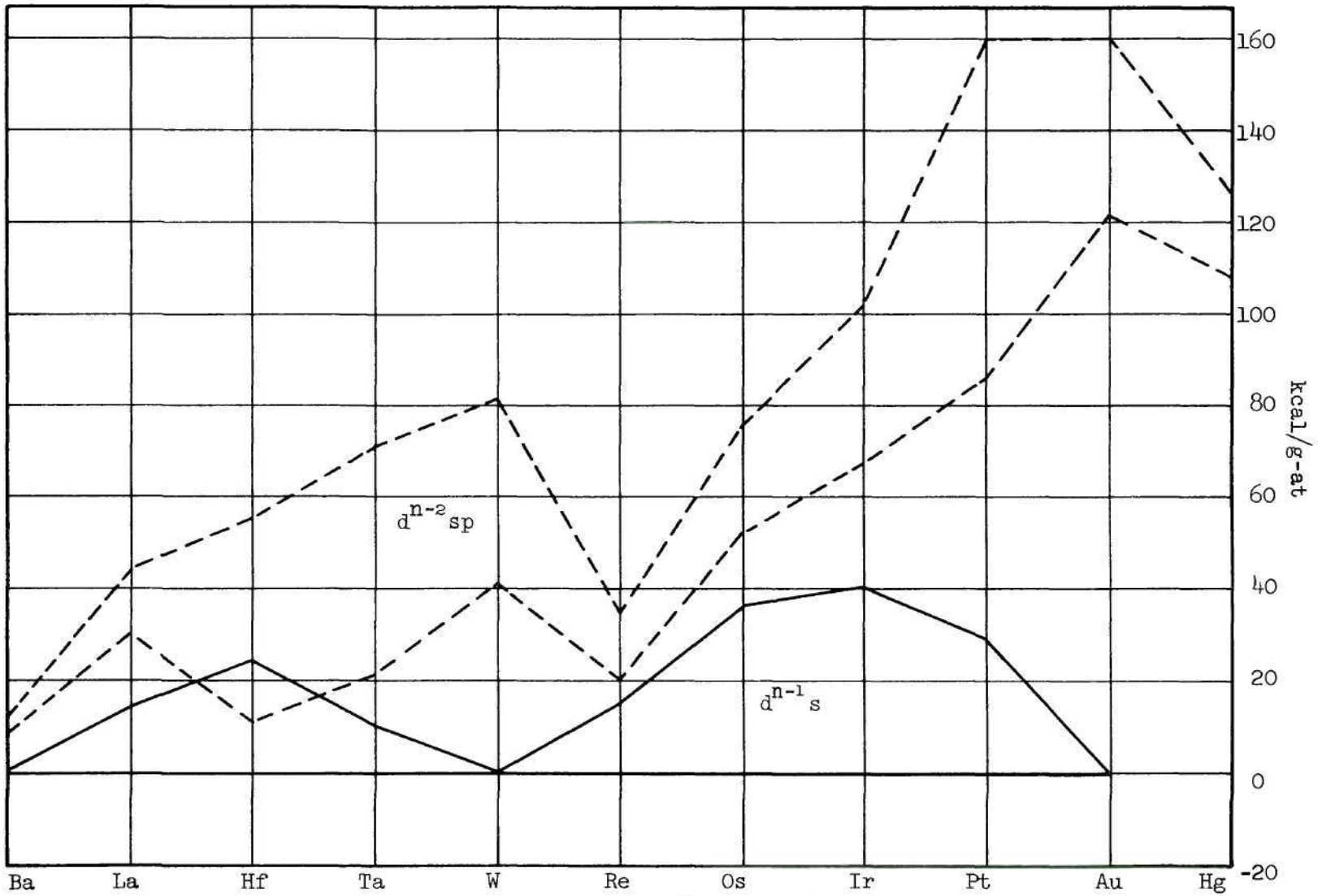

Figure 30. Relative Promotion Energy of $d^{n-1}s$ and $d^{n-2}sp$ Electronic Configurations for the Sixth Period Elements

between the outer shell and the inner shell when external stress is applied. This fact is consistent with the experimental results that there are smaller internal energy changes per unit strain in Ti, Zr, and Hf due to stressing than that of the sixth column, as shown in Figures 25, 26, and 27. It is also in agreement with the assumption that the atomic size of these elements is controlled by both s+p electrons and d electrons, and the electron movements between outer shell and inner shell could be expected by stressing. For the fifth and sixth columns in three transition element periods, such as V, Cr, etc., it can be seen that the electronic configuration $d^{n-2}sp$ is so highly promoted compared to the configuration with only one s electron that one would predict the hcp structure to be very unstable compared to the bcc structure and the opportunities of electron transfers between the outer shell and the inner shell would be very few. This again is in agreement with greater internal energy change per unit strain in our experiments. The right side of the sixth column in three transition element periods shows approximately the reversed tendency.

In the nontransition metals, such as Be, Mg, Al, Sn, and Pb, there is either no d shell existing or the d shells are filled. No electron transfer should be expected in these metals. Should there be electron transfer to higher levels, the promotion energy would be very high. It is in agreement with the high experimental value in internal energy change per unit strain.

CHAPTER VI

CONCLUSIONS AND RECOMMENDATIONS

From this investigation it may be concluded that:

1. The calculated thermoelastic effect is in reasonable agreement in the experiments for all elements except zinc, as shown in Figures 22 through 24 and Table 3.

2. The energy change calculated from the measured variation of temperature is much larger than the work done on the specimens in stressing. The ratio $\Delta H/\Delta W$ varies from 2.5 to 52.

3. The change of internal energy per gram atom and unit stress is greatest for normal elements and decreases towards the middle of the transition metals.

4. The change of internal energy per gram atom and unit strain varies irregularly over the periodic chart. It is highest for the normal metals. Among the transition elements minima seem to exist around the fourth, fifth column and the ninth, tenth column elements when shells are almost half filled and completed, as shown in Figure 26. This change over the periodic chart may be related to the similar change of Poisson's ratio over the periodic chart.

5. Because of the difficulties of calculating the atomic vibrational energy change with stress or strain in solid state, the contribution of atomic vibrational energy to internal energy change due to

stressing is rather uncertain. The change in internal energy is partly due to atomic vibrations and partly due to electronic promotions. These two variables cannot be separated in the present investigation. It is the hope that the atomic vibrational energy can be obtained and further conclusions can be made when the data of the internal energy change due to compression are available.

The following recommendations are made for further work:

1. The work should be extended to the influence of compression on electron transfer between the outer and the inner shells.

2. The investigations should be extended to a series of alloy systems in which magnetic transformation cross transition temperatures or regions of large damping capacity exist. Investigation of compounds of different bonding patterns may yield interesting information. Metastable phases such as martensites would be of interest.

3. Special work should be undertaken to determine the influence of stress on atomic vibrational energy.

4. Work should be done to determine the influence of frequency of stressing.

APPENDICES

APPENDIX I

CALIBRATION OF OVERSHOOT OF THE AMPLIFIER

Since the amplifier works with an input transformer and a chopper, a calibration for overshoot due to low frequency is needed. The calibration was done by comparing the differences of the deflection between a steady given dc and low frequency input of the same voltage. The low frequency input was obtained by the output of the strain gauge circuit on the spring of a given dc power supply when the punch press machine was running. The dc input on the amplifier of a given dc was achieved when the punch press machine was setting on the maximum load. In this way, the same potential was applied on the amplifier for both dc and low frequency inputs. Usually, the deflections were measured under maximum load on both dc and low frequency inputs of the same voltage. From these deflections, the percentage of overshoot was determined. The calculation of the calibration of overshoot was made as follows:

For the gain range of amplifier, 0.03 mv

galvanometer used: M40-350A

deflection of low frequency input = 14.54 cm

deflection of dc input = 14.30 cm

difference between above two values = 0.24 cm

percentage of overshoot in full scale

$$= \frac{\text{difference between low frequency and dc}}{\text{deflection of dc input}}$$

$= 0.24/14.30 = 1.7\%$.

APPENDIX II

CALCULATIONS OF TEMPERATURE CALIBRATION

As shown in Figure 13, the voltage on the calibration box was measured by a Leeds & Northrup potentiometer. The potential over the four standard one ohm resistors could be calculated very accurately. This known small potential was applied on the input of the amplifier. The deflection corresponding to the known potential was recorded on the visicorder by galvanometer M40-350A. Then the conversion factor of deflection in centimeters on the visicorder to the potential was obtained. In this way, the temperature of a given thermoforce can be determined. The simple calculation was given as follows:

For the gain range on amplifier, 0.03 mv

voltage on calibration box = 1.0528 volts

voltage over the four standard one ohm resistors

$$= \frac{1.0528 \times 4}{260,000}$$

$$= 16.2 \times 10^{-6} \text{ volts}$$

deflection measured on the visicorder graph was 13.4 cm

corresponding to 16.2×10^{-6} volts

conversion factor of deflection in centimeters to potential

$$= \frac{16.2 \times 10^{-6}}{13.4}$$

$$= 1.209 \times 10^{-6} \text{ volts/cm.}$$

In these experiments, the chromel and constantan thermocouples were used.

From the thermocouple calibration tables, the thermoforce changes are 0.61 millivolt between 20°C and 30°C. Then

conversion factor of deflection in centimeters to degree centigrade $= \frac{1.209 \times 10^{-6} \times 10}{0.61 \times 10}$

$= 0.0198$ °C/cm.

APPENDIX III

TYPICAL CALCULATION OF INTERNAL ENERGY CHANGE

The calculation of internal energy change of yttrium is illustrated as an example. In our experiment, the internal energy change was expressed per unit stress and unit strain for the convenience of comparison. The calculations for both cases are shown as follows:

Given:

atomic weight = 88.9

Young's modulus, $Y = 0.661 \times 10^6$ kg/cm^2

specific heat, $C = 0.0714$ cal/g/°C = 6.34 cal/g-at/°C

density, $d = 4.47$ g/cm^3

cross section of the specimen = 0.130 cm^2

conversion factor of deflection in cm to the load in kg

= 6.828 kg/cm

conversion factor of deflection in cm to the temperature

in degrees centigrade = 0.0198 °C/cm

deflection of maximum load in cm = 17.4 cm

deflection of temperature change = 16.03 cm

Calculation:

maximum load on the specimen = $17.4 \times 6.828 = 122$ kg

stress on the specimen = $\frac{122}{0.130}$

= 940 kg/cm^2

temperature variation = 16.03 x 0.0198

= 0.318 °C

$$\frac{\text{temperature variation}}{\text{stress variation}}, \frac{\Delta T}{\Delta \sigma} = \frac{0.318}{940}$$

$= 3.38 \times 10^{-4}$ °C/kg/cm^2

For the unit stress, assume $\Delta\sigma = 1{,}000$ kg/cm^2 and the length of the specimen is one centimeter.

Heat energy change, $\Delta H = m^* \times C \times T$

$= 6.34 \times 3.38 \times 10^{-4} \times 1000$

= 2.15 cal/g-at.

$$\Delta l = F \frac{l}{YA}$$

$$= 122 \times \frac{l}{0.661 \times 10^6 \times 0.130}$$

$= 1.23 \times 10^{-3}$ cm $= 1.23 \times 10^{-5}$ m

Work done on the specimen, $\Delta W = \frac{1}{2} F \Delta l$

$$= \frac{\frac{1}{2} \times 122 \times 9.8 \times 1.23 \times 10^{-5}}{0.130 \times 1 \times 4.47}$$

$= 12.65 \times 10^{-3}$ joule/gm

$$= \frac{12.65 \times 10^{-3} \times 88.90}{4.18} \text{ cal/g-at}$$

= 0.266 cal/g-at.

Internal energy change, $\Delta E = \Delta H - \Delta W$

= 2.15 - 0.266

= 1.88 cal/g-at

$\Delta H/\Delta W = 2.15/0.266$

= 8.07.

For the unit strain, assume $\Delta l/l = 10^{-3}$ and the length of the specimen = 1 cm.

---

*unit mass equal to one

Stress on the specimen, $\Delta\sigma = Y \frac{\Delta l}{l}$

$= 0.661 \times 10^{6} \times 10^{-3}$

$= 0.661 \times 10^{3}$ kg/cm^2

Temperature variation, $\Delta T = 3.38 \times 10^{-4} \times 0.66 \times 10^{3}$

$= 0.223$ °C

Heat energy change, $\Delta H = m \times C \times \Delta T$

$= 6.34 \times 0.223$

$= 1.417$ cal/g-at

Cross section of the specimen for getting the stress,

0.661×10^{3} kg/cm^2 $= \frac{122}{0.661 \times 10^{3}}$

$= 0.185$ cm^2

Work done on the specimen, $\Delta W = \frac{1}{2} F \Delta l$

$= \frac{\frac{1}{2} \times 122 \times 9.8 \times 10^{-5}}{0.185 \times 1 \times 4.47}$

$= 7.23 \times 10^{-3}$ joule/gm

$= \frac{7.23 \times 10^{-3} \times 88.9}{4.18}$ cal/g-at

$= 0.154$ cal/g-at

Internal energy change, $\Delta E = \Delta H - \Delta W$

$= 1.417 - 0.154$

$= 1.263$ cal/g-at

$\Delta H/\Delta W = 1.417/0.154$

$= 9.22$

Table 1. Calibration of Load on the Spring*

Load (kg)	Deflection (cm)	Load/Deflection (kg/cm)
27.13	4.05	6.70
52.64	7.79	6.75
78.01	11.41	6.83
103.20	14.90	6.92
124.97	18.02	6.94
103.20	14.90	6.92
78.01	11.41	6.83
52.64	7.79	6.75
27.13	4.05	6.70
	Average	6.828

*The calibration was made under potential on the Wheatstone bridge being 3.50 volts.

Table 2. The Yield Strength (19), Diameter, and Stress on the Specimens

Elements	Specimen Index #	Yield Strength (kg/cm^2)	Diameter (cm)	Stress on Specimen (kg/cm)
4 Be	37	1,900 - 2,670	0.627	395*
12 Mg	10		0.515	587
13 Al	7	1,080	0.472	697
22 Ti	24	1,600	0.320	1,520
	26	1,600	0.397	984
23 V	12	4,480	0.318	1,540*
	13		0.479	678
26 Fe	22	2,110	0.316	1,555
27 Co	38	7,800	0.643	376*
28 Ni	29	600	0.602	427
29 Cu	5	1,050	0.400	973
	6		0.478	690
30 Zn	34	1,330	0.633	388*
39 Y	8	980	0.322	940
40 Zr	21	4,950	0.476	686*
41 Nb	19	2,810	0.359	1,205
	18		0.240	2,700
42 Mo	23	5,270	0.316	1,555*
45 Rh	30		0.634	386
46 Pd	32	1,400	0.638	381*
	33		0.438	747
47 Ag	35	650	0.508	603
48 Cd	39		0.630	389
50 Sn	40	99	1.263	97

Table 2. The Yield Strength (19), Diameter, and Stress on the Specimens (Concluded)

Elements	Specimen Index #	Yield Strength (kg/cm^2)	Diameter (cm)	Stress on Specimen (kg/cm)
72 Hf	14	2,320	0.318	1,540
	15		0.477	685
73 Ta	16	4,930	0.318	1,540*
	17		0.477	685
	20		0.573	473
74 W	42	10,300	0.317	1,555*
79 Au	36	2,100	0.636	384*

*It is due to the difficulties in specimen preparations that the stress on those elements is much lower than the yield strength.

Table 3. Observed and Calculated Values of $\Delta T/\Delta\sigma$

Li	Be 1.055 0.995											B	C
Na	Mg 4.620 4.240	Al 3.450 2.770									Mg	Al	Si
K	Ca 6.510	Sc 1.726	Ti 1.204 1.166	V 1.020 0.822	Cr 0.759	Mn 1.850	Fe 1.066 0.967	Co 1.100 0.973	Ni 1.112 0.937	Cu 1.550 1.417	Zn 2.840 3.120	Ga	Ge
Rb	Sr 7.510	Y 2.627	Zr 1.040 0.924	Nb 1.010 0.900	Mo 0.662 0.576	Tc 0.837	Ru 0.921	Rh 1.025 0.810	Pd 1.355 1.146	Ag 2.255 2.260	Cd 4.840 4.470	In	Sn 3.56 3.82
Cs	Ba 7.920	La 2.614	Hf 1.042 0.923	Ta 0.900 0.817	W 0.573 0.527	Re 0.667	Os 0.465	Ir 0.646	Pt 0.917	Au 2.080 1.660	Hg	Tl	Pb 5.69 5.77

Note: The numerical entry below the symbol of an element gives values for observed $(\Delta T/\Delta\sigma) \times 10^{-4}$, °C/kg/cm^2. Where a second entry is given, it is for the calculated $(\Delta T/\Delta\sigma) \times 10^{-4}$, °C/kg/cm^2.

Table 4. Coefficients of Thermal Expansion (19), Atomic Volume (19), and Specific Heat (20)

Element	$\alpha \times 10^6$ ($°C^{-1}$)	Atomic Volume (cm^3/g-at)	Specific Heat (cal/g-at/°C)
4 Be	11.5	4.891	3.93
12 Mg	25.7 ± 0.7	14.00	5.92
13 Al	23.1 ± 0.5	10.00	5.82
22 Ti	8.35 ± 0.15	12.01	5.98
23 V	8.3	8.365	5.905
24 Cr	8.4	7.231	5.57
26 Fe	11.7	7.094	5.98
27 Co	12.4	6.689	5.95
28 Ni	12.7 ± 0.2	6.593	6.23
29 Cu	16.7 ± 0.3	7.114	5.855
30 Zn	29.7	9.165	6.07
39 Y	12.0	19.88	6.34
40 Zr	5.78 ± 0.07	14.02	6.12
41 Nb	7.07 ± 0.05	10.83	5.965
42 Mo	4.98 ± 0.15	9.387	5.695
45 Rh	8.40 ± 0.10	8.292	6.00
46 Pd	11.5 ± 0.4	8.879	6.21
47 Ag	19.2 ± 0.4	10.27	6.095
48 Cd	30.6 ± 1.3	13.00	6.215
50 Sn	21.2	16.30	6.30
72 Hf	6.01 ± 0.16	13.45	6.10
73 Ta	6.55 ± 0.05	10.80	6.07
74 W	4.59 ± 0.03	9.551	5.84
79 Au	14.1 ± 0.1	10.22	6.065
82 Pb	29.0 ± 0.3	18.27	6.39

Table 5. Changes of Heat Energy and Internal Energy in the Specimens

Li	Be 0.407 0.386 1.000											B	C
Na	Mg 2.746 2.385 1.120	Al 2.000 1.803 1.191									Mg	Al	Si
K	Ca	Sc	Ti 0.717 0.611 0.698	V 0.619 0.547 0.752	Cr	Mn	Fe 0.655 0.622 1.140	Co 0.657 0.654 1.220	Ni 0.684 0.649 1.288	Cu 0.907 0.833 0.666	Zn 1.698 1.585 1.495	Ga	Ge
Rb	Sr	Y 2.150 1.880 1.260	Zr 0.635 0.442 0.452	Nb 0.608 0.504 0.607	Mo 0.418 0.385 1.020	Tc	Ru	Rh 0.622 0.590 1.575	Pd 0.842 0.751 0.924	Ag 1.358 1.190 0.960	Cd 2.993 2.720 1.599	In	Sn 0.228 0.227 1.152
Cs	Ba	La	Hf 0.653 0.539 0.689	Ta 0.553 0.486 0.810	W 0.349 0.317 0.827	Re	Os	Ir	Pt	Au 1.278 1.130 0.946	Hg	Tl	Pb 0.364 0.363 0.547

Note: The first numerical entry below the symbol of an element gives the value for $\Delta H/\Delta\sigma$, cal/g-at/unit stress; the second, ΔE, cal/g-at/unit stress; the third, ΔE, cal/g-at/unit strain.

Table 6. Promotion Energies of $d^{n-2}sp$ Valence State (in kcal per mole)

Ground-state configurations										
s^2	ds^2	d^2s^2	d^3s^2 except*	d^5s except*	d^5s^2	d^6s^2 except*	d^7s^2 except*	d^8s^2 except*	$d^{10}s$	$d^{10}s^2$
Mg 63										
Ca 43	Sc 45-46,53	Ti 45-54,72-80	V 47-54,81-88	Cr 71-80	Mn 53	Fe 55-70	Co 67-76	Ni(d^8s^2) 74-87	Cu 113-128	Zn 92-94
Sr 41-43	Y 43-49,54	Zr 42-57,66-74	Nb*(d^4s) 48-61,74-86	Mo 80-93	Tc 47-50	Ru*(d^7s) 72-93	Rh*(d^8s) (95)-	Pd*(d^{10}) <145-	Ag 161-185	Cd 86-91
Ba 35-39	La 38-40,50-52	Hf 51-79,85-95	Ta 49-99	W*(d^4s^2) 49-99	Re 54-68	Os 67-(90)	Ir 75-109	Pt*(d^9s) 86-160	Au 121-160	Hg 108-126
Ra 37-48	Ac 39-68									

Table 7. Promotion Energies of $d^{n-1}s$ Valence State (in kcal per mole)

Ground-state configurations									
s^2	ds^2	d^2s^2	d^3s^2 except*	d^5s except*	d^5s^2	d^6s^2 except*	d^7s^2 except*	d^8s^2 except*	$d^{10}s$
Mg 137									
Ca 58	Sc 33,51	Ti 19,40	V 6-7	Cr 0	Mn 49-50	Fe 20-23,50-51	Co 10-15,43-46	Ni 1-5	Cu 0
Sr 52	Y 31-33,44	Zr 14-17,31-32	Nb*(d^4s) 0-3	Mo 0	Te 7-12	Ru*(d^7s) 0-9,25-27	Rh*(d^8s) 0-10,26-31	Pd*(d^{10}) 10-29	Ag 0
Ba 26-27	La 8-12,21-22	Hf 40-51,59-64	Ta 28-38	W*(d^4s^2) 8	Re 34-49	Os 15-37,44-(51)	Ir 8-34,37-48	Pt*(d^9s) 0-29	Au 0
Ra 37-42	Ac (15-20),26-35								

BIBLIOGRAPHY

1. Born, Handbuck der Physik XXXIV 12.

2. Madelung, E., Zeits fur Physik 11 (1910) 898.

3. Hume-Rothery, W., Atomic Theory for Students of Metallurgy, Institute of Metals, London 1948.

   Hume-Rothery, W., The Structure of Metals and Alloys, Institute of Metals, London 1936.

4. Lewis, G. N., Journal of the American Chemical Society 38, 762 (1916).

5. Lewis, G. N., Die Valenz und der Bau der Atome und Molekule, Vieweg & Sohn, Braunochweig 1927.

   Journal of Chemical Physics 1 (1932) 17.

6. Drude, P., Ann Physik 1 (1900) 566; 3 (1900) 370; 7 (1902) 687.

   Lorentz, H. A., Proc. Acad. Amsterdam 7 (1905) 438, 585, 684.

7. Sommerfeld, A., Zs. Physik 47 (1928) 1.

   Sommerfeld, A. and Bethe, H., Elektronentheorie der Metalle, Handbuck der Physik, vol. 24/2 (1933) 333.

8. Block, F., Zeits. fur Physik 52 (1928) 555; 59 (1930) 208.

9. Seitz, F., The Modern Theory of Solids, McGraw-Hill Book Company, Inc., New York 1940.

10. Pauling, L., The Nature of the Chemical Bond, Third Edition, Cornell University Press, Ithaca 1960.

11. Mott, N. F. and Jones, H., The Theory of Properties of Metals and Alloys, Clarendon Press, Oxford 1936.

12. Brewer, Leo, Prediction of High Temperature Metallic Phase Diagrams, UCRL-10701, University of California, July 1963.

    Brewer, Leo, "Thermodynamic Stability and Bond Character in Relation to Electronic Structure and Crystal Structure," Electronic

Structure and Alloy Chemistry of the Transition Elements, Interscience, New York 1963.

13. Heisenberg, W., Zeitschnift fur Physik 33 (1925) 879.

14. Schrodinger, E., Annalen der Physik 79 (1926) 361, 489, 734; 80, 437; 81, 109.

15. Engel, N., Kemisk Maanedsblad 30 (1949) 53, 97.

Engel, N., Das Kubisch raumzentrierte Gitter als Einelektronphase, "Radex-Rundschau," Heet 3, 1956.

16. Engel, N., Energy Wave Hypothesis, in print.

17. Engel, N., "Metallic Lattices Considered as Electron Concentration Phases," ASM Transactions Quarterly, vol. 57, No. 3, September (1964).

Engel, N., "Copper, Copper Alloys and the Electron Concentration Concept," ACTA Metallurgica, vol. 15, March 1966.

18. Rocca, Roberto and Bever, M. B., "The Thermoelastic Effect in Iron and Nickel as a Function of Temperature," Transactions AIME, Vol. 188, February (1950).

19. Karl, A. Gschneidner, Jr., "Physical Properties and Interrelationships," Solid State Physics 16 (1964).

20. American Society for Metals, "Properties and Selection," Metal Handbook 1 (1961).